Energy Conversion and Management: X 23 (2024) 100589

Contents lists available at ScienceDirect

Energy Conversion and Management: X

journal homepage: www.sciencedirect.com/journal/energy-conversion-and-management-x

Deoxygenation of waste sludge palm oil into hydrocarbon rich fuel over carbon-supported bimetallic tungsten-lanthanum catalyst

A. Afiqah-Idrus [a,d], G. Abdulkareem-Alsultan [a,b,d,*], N. Asikin-Mijan [c,1], Maadh Fawzi Nassar [a,d], Lee Voon [f], Siow Hwa Teo [a,e], Tonni Agustiono Kurniawan [g], Nur Athirah Adzahar [a], M. Surahim [a], Siti Zulaika Razali [h], Aminul Islam [i], Robiah Yunus [b], Noor Alomari [j], Yun Hin Taufiq-Yap [a,d,*,1]

[a] Catalysis Science and Technology Research Centre, Faculty of Science, Universiti Putra Malaysia, Serdang 43400, Malaysia
[b] Department of Chemical and Environmental Engineering, Universiti Putra Malaysia (UPM), 43400 Serdang, Selangor, Malaysia
[c] Department of Chemical Sciences, Faculty of Science and Technology, Universiti Kebangsaan Malaysia (UKM), 43600 Bangi, Selangor Darul Ehsan, Malaysia
[d] Department of Chemistry, Faculty of Science, Universiti Putra Malaysia, 43400 UPM Serdang, Selangor, Malaysia
[e] Industrial Chemistry Program, Faculty of Science and Natural Resources, Universiti Malaysia Sabah, 88400 Kota Kinabalu, Sabah, Malaysia
[f] Nanotechnology and Catalysis Research Centre (NanoCat), Institute of Postgraduate Studies, University Malaya, 50603 Kuala Lumpur, Malaysia
[g] College of the Environment and Ecology, Xiamen University, Xiamen 361102, Fujian, China
[h] Institute of Nanoscience and Nanotechnology, Universiti Putra Malaysia, Serdang, Seri Kembangan 43400, Selangor, Malaysia
[i] Department of Petroleum and Mining Engineering (PME), Jashore University of Science and Technology, Jashore 7408, Bangladesh
[j] Department of Chemical and Paper Engineering, Western Michigan University, Kalamazoo, MI 49008, USA

ARTICLE INFO

Keywords:
In situ mechanism
In situ XAS
In situ FTIR
Heterogeneous catalysis
Green-diesel
Activated carbon
Deoxygenation

ABSTRACT

Activated carbon (AC) supported catalysts have been extensively applied as deoxygenation (DO) catalysts. However, the details of in situ experimental investigations that relevant to this catalyst are limited. Hereby, we present a series of operando/in situ spectroscopic experiments for DO of waste sludge palm oil (WSPO) by using atomically dispersed La-W bimetallic supported AC catalysts (La-W/AC) with well-defined structures. The $La_{(5\%)}$-$W_{(2\%)}$/AC catalyst prepared through co-precipitation (CP) process rendered high surface area (741 m^2/g) and catalyst's acidity (13319.16 μmol/g). Besides, the catalyst demonstrated a superior catalytic performance of DO reactivity under optimal reaction conditions of 0.5 % catalyst loading (CL), a one hour reaction time (Rt), and 250 °C reaction temperature (RT), achieving 98 % WSPO conversion to green fuel turnover frequency (TOF) of 0.0153 s-1. The reusability of $La_{(5\%)}$-$W_{(2\%)}$/AC catalyst was positively active for eight runs of DO process with constant of conversion rate at > 87 %. In addition, DO mechanism was of WSPO model compound (palmitic acid) was conducted to gain the clearer insight of reaction pathway catalysed by La-W/C catalyst. In situ FTIR analysis confirms the presence of intermediates (e.g. n-heptadecane, n-pentadecane, n-nonane, n-tridecane, and trimethylcyclopentene) that attributed buy the acid site of the heteropoly acid support. Besides, in situ XAS spectroscopy consolidates the oxidation state of La and W, where the presence of metal centre, support and substrate were confirmed to reflect the occurrence of palmitic acid DO on atomically dispersed La and W active sites. Thus, the present findings identified several key product intermediates during DO process, as well as the stable-state of catalyst structure, which suggest that the atomically dispersed $La_{(5\%)}$-$W_{(2\%)}$/AC catalysed reactions follow an unconventional decarboxylation/decarbonylation reaction pathways with the activation of oxygen (O_2) removing is rate limiting.

* Corresponding authors at: Catalysis Science and Technology Research Centre, Faculty of Science, Universiti Putra Malaysia, Serdang 43400, Malaysia (A.G. Abdulkreem Alsultan); Catalysis Science and Technology Research Centre (PutraCAT), Chemistry Department, Faculty of Science, Universiti Putra Malaysia, 43400, Selangor, Malaysia (Y. Hin Taufiq-Yap).
E-mail addresses: kreem.alsultan@yahoo.com (G. Abdulkareem-Alsultan), nurul.asikin@ukm.edu.my (N. Asikin-Mijan), taufiq@upm.edu.my (Y. Hin Taufiq-Yap).
[1] The two authors have the same contribution to this study.

https://doi.org/10.1016/j.ecmx.2024.100589
Received 25 January 2024; Received in revised form 21 March 2024; Accepted 8 April 2024
Available online 11 April 2024

Introduction

A rise in energy requirements, the exhaustion of fossil fuel sources on a global scale and additional associated environmental issues, i.e. global warming, have stemmed from ongoing use of petroleum-based fuel. This has impelled the scientific population and research workers internationally to identify a superior and more sustainable form of energy from natural resources that would ameliorate the persisting problems linked with fossil-based fuels. The current energy crisis has encouraged scientists to concentrate on the generation of replenishable biofuels which are sustainable and less detrimental to the planet and its ecosystem. However, this strategy is not very selective, in that a spectrum of undesired by-products, essentially oxygenates, necessitates a further development phase in order to eradicate these from green fuel. Well-known biofuels, e.g. biodiesel or fatty acid methyl esters, comprising well-oxygenated complexes, have a number of unavoidable disadvantages, including lack of integrity for long-term storage and suboptimal cold-flow activity [1,2]. Thus, the eradication of oxygen (O_2)-bonded composites is required in order to attain apposite fuel characteristics.

The main drawback associated with biodiesel and bio-oils is their high O_2 concentration, which contributes towards inferior heat properties, when compared with conventional fossil-derived oils. Researchers in this domain are currently focused on the generation of O_2-free hydrocarbon (HC), through the catalytic deoxygenation (DO) of fatty acids and associated compounds. Theoretically, DO involves the elimination of O_2 from biodiesel and bio-oils by way of decarboxylation (–CO_2) and decarbonylation (–CO, H_2O) (deCOx) reactions within an environment devoid of hydrogen (H_2). As green and petroleum-derived diesels both come with similar physicochemical properties, the former can be utilized individually, or together with conventional diesel, for combustion ignition engines, without the need for any alterations to the engine.

Businesses are attracted to the concept of green diesel, but the expenditure associated with its manufacture is high when contrasted against petroleum-based products. Thus, cost is the predominant impediment to upscaling its production [3]. A recent approach to diminishing the manufacturing expense on a large scale is through the deployment of cheap feedstock, e.g. waste sludge palm oil (WSPO) and low-price catalysts that can be recycled. Studies have indicated that the use of WSPO facilitated a budget reduction of between 60–90 % [4]. Moreover, the increasing worries linked with the environment and the safe treatment and discarding of WSPO have promoted the design of less hazardous waste processes and green fuel that generates no waste products [5,6]. Consequently, the use of WSPO as feedstock for the manufacture of transportation biofuel is an answer to the issues surrounding waste clearance [7,8].

The uncomplicated decontamination phase and recycling potential of a wide variety of solid catalysts, render them favourable for the generation of green fuel [8]. Solid catalysts can be separated into two main categories: (a) the basic category which comprises alkaline-based and alkaline-earth-based metal oxides, and (b) the acid category which includes functionalised silica substances, MCM-41 and SBA-15, with organic-sulphonic acids [9]. Generally, in terms of the DO reaction, the use of solid base catalysts results in milder reactivity in comparison to the use of solid acid catalysts [10]. Nonetheless, WSPO occurs as an acid oil holding great amounts of free fatty acids (FFAs), and the active moieties of the base catalyst applied for the DO reaction, is mostly constrained by the FFAs, due to the effects stemming from the occurrence of a saponification episode [10].

An acid catalyst is considered more effective for the simultaneous DO of FFAs and triglycerides, to derive a single-pot fusion of alkane and alkene from WSPO, at raised reaction temperatures (RTs) [12]. Thus, in the context of green fuel generation from low-grade oil, at cooler RTs, the use of a non-homogeneous solid acid catalyst, can be considered an environmentally friendly, and cost effective option [11–15]. The mild reaction issue is the main stumbling block, to the realization of an effective solid acid catalyst, for the DO reaction.

The emphasis of previous studies associated to deCOX was on the palladium (Pd)-supported and platinum (Pt)-supported catalysts, which portrayed favourable transformation capacities for diesel-type HCs [7,10–21]. However, the high cost of these precious metals, hampers their usage on a commercial scale. Lower cost carbon C-based catalysts, on the other hand, deliver almost similar outcomes to those associated with the Pd-linked and Pt-linked compounds, for the transformation of lipid-based feeds into fuel-type HCs [22,23].

The C-based catalysis of triglycerides and its associated composites to green fuel is the topic of a contemporary review [24]. The reasonable transformations and discrimination of the DO reaction attained on C-based catalysts combined with metal oxide adjuncts is owing to their large surface area and integrity at high RTs [25–27]. In fact, during deCOx reactions, catalysts supported by C generally give rise to higher harvests owing to a preferential adsorption of FFA on their surface [28]. Nevertheless, deCOx catalysts are vulnerable to becoming defunct through the surface accretion of carbonaceous materials [13,15,16,29–32]. Self-regeneration can be achieved by utilising high coke formation resistance metal oxides.

Many studies have focused on sulphonated activated carbon (AC) as a catalyst for a spectrum of reactions [18,19], since these materials are extremely stable and have enough protonic acid loci [18]. Activated carbon (AC) obtained from waste biomass is a characteristic cost-effective meso- and macro-porous green support [12]. Active metal oxide C support engagement can enhance the physicochemical traits of a C-founded support catalyst, i.e. consistency, pH, recyclability, and its structural soundness [19]. Nevertheless, the AC remain ineffective for DO reaction. Former studies discovered that addition of binary metal supported on the activated carbon could promoted DO owing by synergistic interaction between the two metals. Based on aforementioned discussion, herein the aims of this study to investigate the synthesis and characterized the binary La-W supported on AC derived from the palm oil mesocarp fibre for promoting effective DO of high FFA WSPO to green fuel. The La and W as an active element was selected to improve the acid base properties for the catalyst in the deoxygenation reaction the basic properties is important to avoid the coke formation and work as a self regeneration while the acid properties from the W is beneficial to do the cracking of the functional group in the free fatty acid (O-C = O) [20,21]. Outstanding transformation was observed in mild reaction circumstances. The manufactured catalyst's physicochemical characteristics, together with the consequences of a range of reaction variables, i.e. catalyst loading (CL), RT, and Rt, on the green fuel were evaluated. The association between catalytic activity and the surface basicity and acidity of the novel La-W/AC catalyst, in addition to its recyclability, were also explored.

Materials and methods

Materials

Merck (Germany) was the source for lanthanum nitrate hexahydrate (La $(NO_3)_3{\cdot}6H_2O$) with 99.0 % purity, while J.T Baker (USA) was the source for phosphoric acid (H_3PO_4) with 85.0–87.0 % purity. Also acquired from Merck was phosphotungstic acid (H_3PO_4 $12WO_3$ xH_2O) with 99.99 % purity. As the liquid products used are alkane and alkene, we employed the liquid standard of *n*–(C_7–C_{20}) for gas chromatograph analysis, and the internal standard (1-bromohexane). Sigma Aldrich was the source for all the liquid standards, which were used without additional purification measures. GC grade n-hexane with purity > 98 % (Merck, Germany) was utilized for the dilution process. Linde Sdn. Bhd. Malaysia was the source for nitrogen (N_2) gas (99 % pure), while the WSPO utilized as the feedstock for this undertaking, was acquired with the co-operation of the Malaysian Palm Oil Board. The WSPO used for the reaction was not subjected to any purification measures. Table S1 exhibits the physico-chemical properties of the crude WSPO.

Catalyst preparation

Palm pressed fibre (PPF) was used as a source of palm-based AC powder production. In this study, the hot water was used to wash, eliminate dirt and other impurities from PPF prior for drying process (Scheme 1). The pulverisette 4 vario-planetary mill was employed to grind the dried PPF for a three-hour period, with the primary disk and planet pair set at 1200 rpm and 700 rpm respectively. The filtering of the powdered PPF, using a metal sieve of 200 μm (Laboratory test sieve Endecotts Ltd.), was followed by the carbonisation process at 400 °C under the N_2 flow, in a closed furnace, for a four-hour period. Following carbonisation, the sample was subjected to chemical activation using H_3PO_4, in a reflux heating at a RT of 168 °C, for a twelve-hour period. Hot distilled water was used for the purification of the chemically AC powdered sample, until the solution arrived at a pH of 7. The palm-based AC powder was then subjected to drying in an oven set at 100 °C for a two-hour period, followed by doping on the prepared AC, with a precise quantity of lanthanum (La) 1-10 wt% and tungsten (W) 0.5-8 wt% nanoparticles, by way of the hot injection procedure [22,23]. The synthesis was executed in a Schlenk line setup, in a 250 mL flask. A vacuum was applied to purge the reaction mixture (0.4 mL oleic acid, 0.4 mL oleylamine, 6.86 mg 1,2-hexadecanediol, and 20 mL diphenyl ether), and subsequently charge it with N_2 gas. This process was replicated five times, before the mixture was again degassed under vacuum for a one-hour spell, at a RM of 85 °C. The mixture was then positioned in a N_2 environment, and heated until a RT of 200 °C is arrived at. In the meantime, 5 g of AC was disseminated in dichlorobenzene and merged with the pre-determined quantity of lanthanum nitrate hexahydrate La $(NO_3)_3{\cdot}6H_2O$, and phosphotungstic acid H_3PO_4 $12WO_3$ xH_2O. The mixture was then heated under sonication to 80 °C. Subsequently, the $La_{(5\%)}$-$W_{(2\%)}$/AC mixture was injected into a three-neck flask, and subjected to stirring for a period of 10 min, before being cooled in a water bath. This was followed by the rinsing of the mixture in a three-fold excess of MeOH and centrifuged (3500 rpm, 10 min), for the elimination of the non-reacted chemicals, as well as the non-attached La and W nanoparticles. The supernatant was then taken out, and the consequential $La_{(5\%)}$-$W_{(2\%)}$/AC heterostructure was re-disseminated in toluene solution, to facilitate the occurrence of ligand exchange. Following the ligand exchange process, the decorated La-W bimetals and the AC support were both conveyed to an aqueous environment. 5 g of the AC was disseminated in 50 ml of toluene, while 40 mL of anhydrous MeOH was merged with 0.5 g of 2-mercaptopropionic acid (MPA). NaOH pellets were also added under stirring, up to the point where the pH breached 10.5. The mixture was subsequently precipitated with acetone/MeOH (1:1, threefold excess) twice, during which the new hydrophilic nanocrystals are mixed with toluene (10 mL), and precipitated to do away with the previous ligands (ligand-exchanged nanocrystals are not disseminated). Following drying under N_2 flow, the crystals were disseminated in deionised water. Finally, a 0.45 μm pore filter was utilized to sieve the mixture, and the residual reactants were subjected to evaporation (rotation evaporator ~ 40 °C) and purging with N_2.

Catalyst characterisation

The chemical arrangement and dissemination capacity of the bimetallic-doped AC catalysts, before and after the chemical reaction, were determined with the utilization of an X-ray diffraction (XRD) technique (Shimadzu, model XRD-6000) [24]. A N_2 adsorption/desorption analyser (Thermo-Finnigan Sorpmatic 1990 series), via the Brunauer-Emmet-Teller (BET) procedure, was employed to measure the surface area of the pulverised sample. Also assessed were the pore size and volume distribution of the generated catalyst. For the purpose of eliminating all extraneous unpredictable materials and water from its surface, the catalyst sample was subjected to degassing overnight, at a RT of 150 °C. The analysis was performed under a RT of −196 °C, and a vacuum chamber was employed for the N_2 desorption and adsorption procedures, on the surface of the catalyst [25].

The temperature programmed desorption (TPD) approach was employed, to investigate the acidic and fundamental aspects of the catalyst. A pair of probe molecules, in the form of NH_3 for acid (TPD–NH_3), and CO_2 (TPD–CO_2) for base, were utilised for the procedure, which involved the use of a Thermo-Finnigan TPDRO 1100 model, equipped with a thermal conductivity detector (TCD). Roughly 50 mg of the catalyst was pre-treated with a thirty-minute N_2 gas flow at a RT of 250 °C, followed by the exposure of the catalyst to CO2 gas

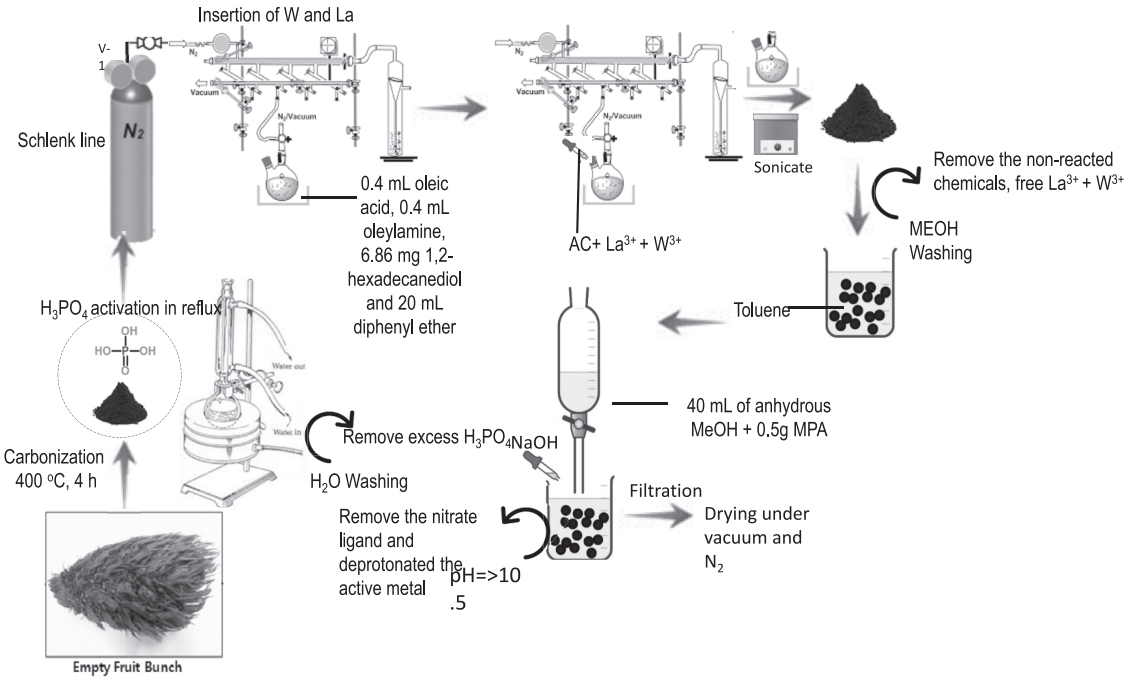

Scheme 1. Research methodology diagram.

adsorption for a period of one hour, at a RT of 50 °C. Subsequently, the TCD was utilized to scrutinize the CO^2 desorption from the catalyst basic locus, using a jet of helium gas at a rate of 30 ml/min, between RTs ranging from 50 °C to 900 °C. The RT was kept at a constant level for a period of 30 min. The adsorption and desorption of NH_3 was then assessed, in accordance with the TDP-CO_2 process [26]. The logging, of the field emission scanning electron microscopy (FESEM) data, was achieved with the use of a LEO 1455 VP.

The analysis of the inductively coupled plasma-atomic emission spectrometry (ICP-AES), for determining the element compositions of the catalyst's specimens (P, W, La and C), was conducted using a Perkin–Elmer Emission spectrometer model Plasma 100 [27]. The chemical states of the $La_{(5\%)}$-$W_{(2\%)}$/AC moiety's surface was assessed by way of X-ray photoelectron spectroscopy (XPS), and the assessments were arrived at via a microprobe PHI quantera II under ultrahigh vacuum settings, specifically at a base vacuum of $\sim 10^{-8}$ Pa, at the ambient temperature.

Mg and Ka ($h\upsilon = 1253.6$ eV) were the X-ray sources employed [28]. Moreover, dedicated analytical equipment for thermogravimetric analysis (TGA 1000i, Instrument Specialists Inc, United States) was utilised to determine the degree of coke and C accumulation on the used catalyst [29]. This method required airflow at a rate of 40 ml/min; de novo and expended catalysts were warmed through a spectrum of RTs i.e. from 25 to 900 °C at a speed of 30 °C/min [30,31].

Catalytic activity evaluation

WSPO deoxygenation was conducted in a 100 ml magnetically agitated batch reactor. For each test, 10 g of WSPO, together with 0.1 g (1 % catalyst to oil ratio) of the catalyst, was introduced into the reactor. Prior to the tests, the reactor was fumigated with inert N_2 flow at 20 cc/min at atmospheric pressure, under constant stirring, to ensure the eradication of O_2, all through the DO reaction, at 250 °C, for a period of one hour. The gas chromatography-flame ionisation detector (GC-FID), Fourier-transform infrared spectroscopy (FTIR), and gas chromatography–mass spectrometry (GC–MS), were utilised for the analysis of the liquid products.

Product evaluation

A Shimadzu GC-14B gas chromatograph (GC), with a HP-5 capillary column length of 30 m, an inner diameter of 0.32 mm, and a film thickness of (25 μm), together with a FID operating at 300 °C, were utilized for appraising the resulting liquid products. Prior to the conversion analysis, the liquid products were diluted with GC grade *n*-hexane, and 1 μL of the specimen. Subsequently, the sample solution was introduced into the GC column, with the injection temperature set at 250 °C, and with N_2 as the carrier gas. The temperature of the oven was initially maintained at 40 °C for six minutes, and then raised to 270 °C at a rate of 7 °C/min. For the quantitative assessments, 1-bromohexane was utilized as an intrinsic reference. The GC-FID analysis of the liquid products facilitates the identification of saturated and unsaturated HC fractions (C_7–C_{20} using the HC reference standard).

The following formula was used to assess the transformation of WSPO and the selectivity of product i (Si):

$$X_{carbon} = \frac{m_i - m}{m_i} \times 100\% \quad (1)$$

where WSPO (feedstock) and the product moles are represented by m_i and m, respectively; the mole of WSPO transformed to product, i.e. *n*-HC and oxygenated intermediates, is given by m.

The second equation states the WSPO turnover frequency (TOF), measured per second:

$$TOF = -\frac{\ln(1 - C_{carbon})}{(\frac{W}{F}) \times D_{CO}} \quad (2)$$

where C_{carbon}, F, W and D_{CO} indicate the conversion, quantity of WSPO placed into the reactor, catalyst weight (g) and CO uptake (mmol/g), respectively.

Since the transformation was above half, which is a long way from selective circumstances, the TOF parameters were assessed using an integral analysis [33]. The $-\ln(1 - C_{carbon})$ expression within the equation is used in place of C_{carbon} and presumes a pseudo first-order reaction. This is apposite to the significant surplus quantity of H_2 and practically isothermal conditions.

The level of data repeatability was determined by performing all the analyses three-fold with 1-bromohexane intensity, which was the intrinsic reference, and a standard deviation < 4. Moreover, the DO liquid products and the non-quantitative assessment of WSPO took place using GC–MS (SHIMADZU QP5050A) apparatus, which incorporated a non-polar DB-5HT column of dimensions 30 m x 0.25 mm x ID μm and an inlet with no splits.

DO liquid product and WSPO dilution occurred following the addition of *n*-hexane (GC grade, i.e. > 98 % pure) to attain a solution of 100 ppm. Confirmation of the fraction peaks of the GC–MS spectrum was conducted by referencing the National Institute of Standards and Testing (NIST) database. Recognition of the principal products necessitated a probability match of ≥ 95 %. The following formula was used to evaluate the distribution of the DO liquid products, namely the HC fractions, carboxylic acid and alcohol:

$$S_{product} = \frac{C_y}{\sum n_y} \times 100\% \quad (3)$$

in which $S_{product}$, C_y *and* n_y represent the yield of organic compounds (%), the area of the ideal organic compounds, and the total area of overall organic compounds respectively.

The Perkin-Elmer Spectrum (PS) 100 spectrometer, used for conducting the FTIR analysis, provides a 4 cm^{-1} resolution, and operates within the 300–4000 cm^{-1} spectrum. This facilitates the identification of the chemical functional residues, associated with the liquid products. The levels of all the metal elements, within the liquid products, were scrutinized by way of ICP-AES analysis.

Results and discussion

Structural characterisations of La-W/AC catalysts

An investigation was conducted on the surface morphology of the La-W/AC catalysts, to ascertain their configuration, pattern and surface particle contours. FESEM images portray a uniform distribution of metal oxides on the AC support (Fig. 1A a–e). Following the doping of the active metals, the measurements and shape of the particles were observed to be markedly altered. It was also noted that the preparation process significantly influences the appearance of the C. An elevation in W content, from 0.5 wt% to 2 wt%, substantially reduced the catalyst's particle size from 1.6 to 1.2 μm. However, an additional elevation in W content to > 2 wt%, increased the particle size from 1.2 to 1.8 μm (Fig. 1A). This development is attributed to aggregation effects. These statistics were further verified through BET and XRD analysis (Fig. 2 and Table 1), which revealed a decrease in surface area and pore volume, together with an expansion in crystal size. The energy dispersive X-ray mapping for the supported catalyst (Fig. 1B), revealed that the distribution of La and W species on the AC surface is unvarying. In addition, bimetallic contents of La and W of La-W/AC catalysts were determined by ICP-AES analysis (Table 1). Results indicated that the bimetallic La-W distributed over the AC support with loading of 1–10 wt% in apposite proportions, i.e. $La_{(5\%)}$-$W_{(0.5\%)}$/AC, $La_{(5\%)}$-$W_{(2\%)}$/AC and $La_{(5\%)}$-$W_{(8\%)}$/AC with strong electrostatic adsorption.

XRD analysis was conducted to identify the crystalline phases of active bimetallic that co-precipitate on the surface of AC. All the catalyst specimens demonstrated a wide diffraction band situated at $2\theta = 20 -$

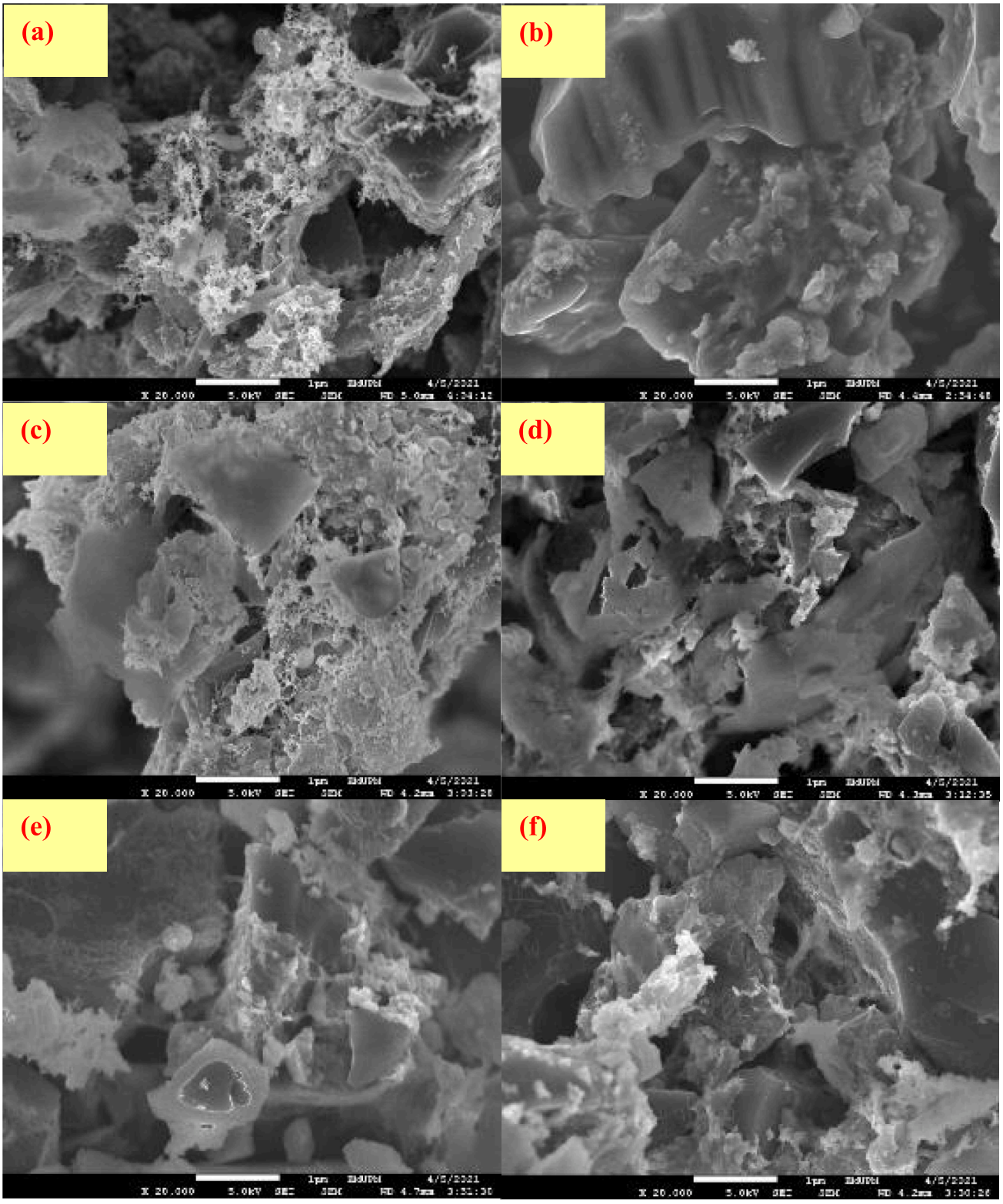

Fig. 1A. FESEM images of (a) $La_{(1\%)}$/AC, (b) $La_{(5\%)}$/AC, (c) $La_{(10\%)}$/AC, (d) $La_{(5\%)}$-$W_{(0.5\%)}$/AC, (e) $La_{(5\%)}$-$W_{(2\%)}$/AC, and (f) $La_{(5\%)}$-$W_{(8\%)}$/AC catalyst.

25°, along with the characteristic of metallics (La, W), metal oxides (La_2O_3, WO_3), and amorphous phases of AC (Fig. 2). Diffraction bands indicating the hexagonal metallic La (La^0) phase were noted at 2θ = 14.95°, 29.99°, 34.64°, 35.01°, 40.83°, 46.23°, 50.58°, 54.18°, 55.97°, 58.32°, 61.57°, 65.01°, 68.13°, and 76.72° (JCPDS: 01–08-92918; ICSD: 04–3573), while the cubic metallic W phases reflecting at 2θ = 18.16°, 38.7°, and 58.44° (JCPDS: 00–0011204). Cubic WO_3 was identified by bands at 2θ = 23.24°, 26.61°, 33.45°, 44.56°, and 72.14° (JCPDS: 00–001-0486); hexagonal La_2O_3 phases were evidenced at 2θ: 25.1°, 28.6°, 30.9°, and 46.2° (JCPDS File No. 01-073-2141; ICSD 024693). The XRD pattern of catalysts with 0.5 wt% W loading demonstrated narrower width and the equivalent crystallite size of La^0 were determined using the Debye-Scherrer formula at 2θ: 29.99°. Clearly, the addition of W species (0.5 wt%) led to the expansion in the crystallite

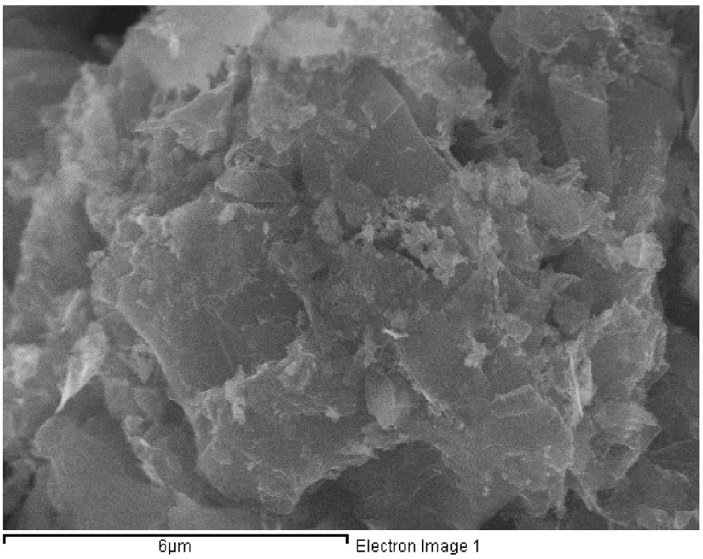

Fig. 1B. Mapping image of La $_{(5\%)}$-W $_{(2\%)}$/AC supported catalyst.

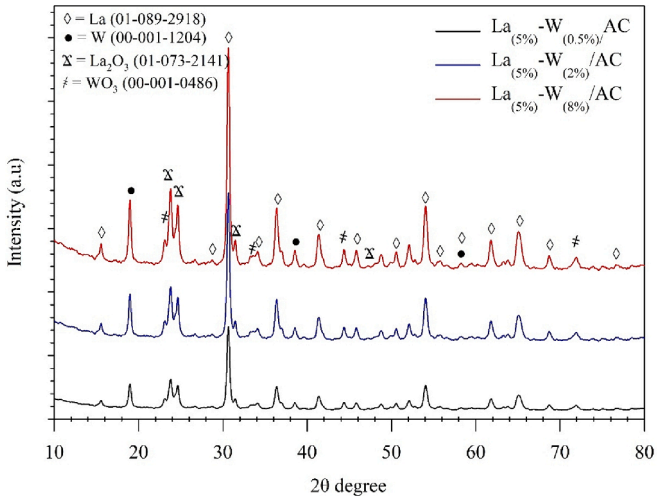

Fig. 2. XRD analysis of La-W/AC catalysts.

dimension of La^0 from 12.5 to 38.0 nm. This is an indication that the growth of the La^0 crystallites, due to the expansion in aggregate particle size, may have led to a decrease in the catalyst surface area. Contrastingly, the La^0 crystallite size is increased by an increase in the W content in the $La_{(5\%)}$-$W_{(2\%)}$/AC catalyst. This is particularly evident for the crystallite size of La^0 with a W loading of 8 wt%, in which the AC catalysts were substantially increased from 29.4 nm (0.5 wt% W) to 38.0 nm (8 wt% W). This is an indication, that the introduction of W into the La^0 lattice decreases the crystallite size, leading to an increase in the catalyst's surface area [32,33].

XPS was employed to evaluate the surface oxidation condition of the active metals (i.e. W and La) of $La_{(5\%)}$-$W_{(2\%)}$/AC catalysts (Fig. 3). As the optimization of acid-base active sites on the $La_{(5\%)}$-$W_{(2\%)}$/AC catalysts is important to enhance the DO activity, thus in-depth investigation of catalysts' surface was performed. Fig. 3a–e shows deconvolution peaks at binding energies (BE) of 284.70–288.61 eV (C); 531.11 – 533.93 eV (O); ~134.65 and 136.33 eV for (P)'; typical zeniths at 36.27 eV and 38.35 eV indicating W $4f^{7/2}$; and 856.49 eV and 838.69 eV reflecting $La3d^5$ (Fig. 3a–e) were observed. Three peaks were exhibited by the O1s spectra for the $La_{(5\%)}$-$W_{(2\%)}$/AC catalysts, i.e. with BE parameters of 531.11, 532.29, and 533.93 eV, respectively (Fig. 3a). In contrast to the reference XPS results from the NIST library, deconvolution demonstrated the O1s narrow scan to be comprised of three O1s constituents [34], implying that the active metal oxides existed in a minimum of three oxidation states within the specimen which could be ascribed to lattice O^{2-} species, O_2^2/O. The BE parameters that were smaller suggested that W(VI) and La(III) oxides situated at 531.11 eV were confirmed; the hydroxyls species, OH^-, was implied by the higher BE constituent, sited at 531.11 eV. The largest zenith, i.e. 533.93 eV, was recognised as surface adsorption of molecular H_2O [35,36]. These data suggest that both La and W are present as oxides on the surface of the catalyst. Notably, the O1s area demonstrated the smallest BE peak in contrast to other elemental species, which are referred as the less electron-rich O_2 species [35,37,38] with just 6 % of O_2 was identified on the $La_{(5\%)}$-$W_{(2\%)}$/AC catalyst. The findings indicated that the $La_{(5\%)}$-$W_{(2\%)}$/AC catalyst predominantly composed of bimetallic La-W alloy on AC support. C1s spectra demonstrated the C within the $La_{(5\%)}$-$W_{(2\%)}$/AC catalyst (Fig. 3b). Four discrete peaks were evident with BE of 284.70, 285.54, 286.98, and 288.61 eV, reflecting C – C, C – O, C = O, and C(O)O moieties, respectively, and thus showing the 3 forms of functional moiety that were encompassed in the synthesis process. The most frequent C1s value was for C – C at 68.39 %, which suggested that the AC support was predominantly made up of C-founded substance containing C – C interaction. The sum of the C content was proportionally high, i.e. 67 % that would improve the thermal stability of the catalyst when exposure to high RTs [39]. Fig. 3c shows the deconvolution curves for W4f, which ranged from 36.27 eV (W4f7/2) to 38.35 eV (W4f5/2), offering proof of the presence of W on the catalyst's veneer. W4′s deconvolution curves implied that the W was spread well on the extrinsic surface of the AC, and it can be postulated that the enhancement of DO catalytic activity is a consequence of the higher distribution of W on the AC [40]. Deconvolution of the high-resolution P2p spectra into a lone zenith is demonstrated at BE of 134.65 eV and 136.33 eV for P2p3/3 and P2p1/2, respectively (Fig. 3d). These data have been associated with the existence of PO_4^{3-} obtained from the antecedent H_3PO_4 utilised for palm-pressed fibre chemical activation [18]. Two BE areas (i.e. 856.49 eV and 838.69 eV) were attributed to La3d5 in La oxide, which indicated the presence of La^{3+} species on the surface of the catalyst [41] (Fig. 3e). In particular, XPS data showed a notable bonding engagement between W^{6+} and La^{3+}, evidenced by a change in the BE of W4f, i.e. from 33.70 (Cos0, standard) to 38.35, together with an alteration in La3d5′s BE from 835.90 eV (La_2O_3, standard) to 838.69 + 0.1 eV [35,42]. The metallic interaction of La and W was confirmed by XRD data (Fig. 2).

Table 1
Physicochemical properties of supported La-W/AC catalyst.

Catalysts	Nominal loading [a] (wt.%)		Actual loading [b] (wt.%, ± 0.9 %)		d_{XRD} [c] (nm)	XRD Composition phases (%) [d]			Specific surface area(SBET) (m^2/g) (±2%)	Pore diameter (nm) (±2%)	Brunauer–Emmett–Teller (BET) Pore volume [e] ($cm^3\ g^{-1}$) (±2%)
	La	W	La	W		La	W	La_2O_3			
$La_{(1\%)}$/AC	1	–	0.8	–	12.5 ± 1.0				914	0.53	0.94
$La_{(5\%)}$/AC	5	–	5.3	–	14.8 ± 0.5				894	0.51	0.87
$La_{(10\%)}$/AC	10	–	10.6	–	16.1 ± 0.9				822	0.48	0.81
$La_{(5\%)}$-$W_{(0.5\%)}$/AC	5	0.5	4.8	0.4	29.4 ± 1.6	33.34	37.31	29.34	785	0.47	0.75
$La_{(5\%)}$-$W_{(2\%)}$/AC	5	2	5.3	1.8	35.3 ± 1.0	56.23	20.13	23.64	741	0.47	0.69
$La_{(5\%)}$-$W_{(8\%)}$/AC	5	8	5.1	8.6	38.0 ± 1.2	50.31	25.39	24.29	980	0.42	0.61

[a] Theoretically calculated;
[b] Deduced from ICP-AES analysis;
[c] Crystallite size (d_{XRD}) calculated from XRD;
[d] Composition deduced from XRD.
[e] Calculated at P/P^0 equal to 0.98.

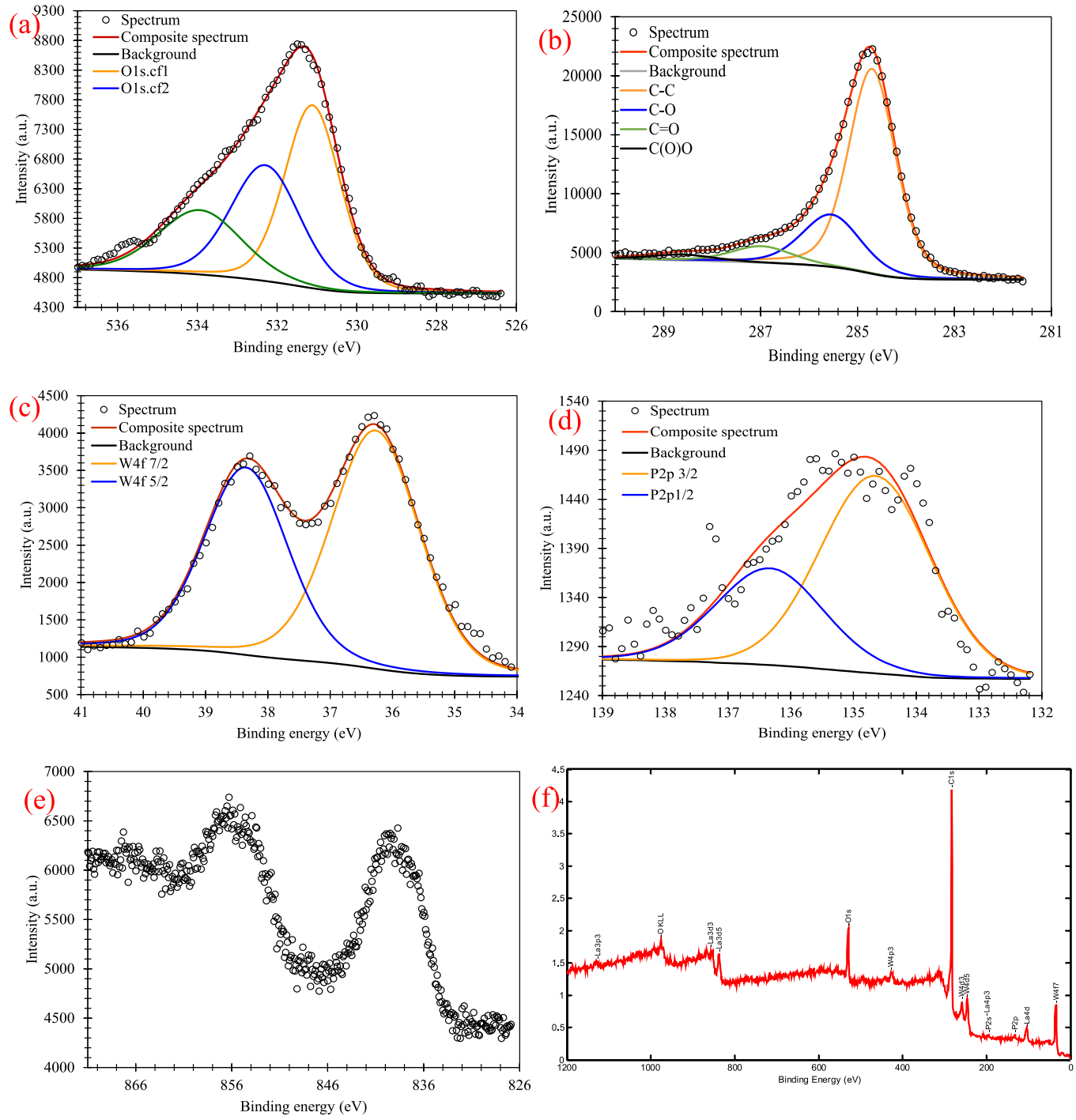

Fig. 3. XPS spectra of (a) O 1 s, (b) C 1 s, (c) Wf4, (d) P 2p, (e) La 3d5 core levels and (f) wide scan for the $La_{(5\%)}$-$W_{(2\%)}$/AC supported catalyst.

Fig. S3 illustrates the N_2 adsorption–desorption isotherms which indicate the textural characteristics and N_2 uptake of $La_{(5\%)}$-$W_{(2\%)}$/AC catalysts. The $La_{(5\%)}$-$W_{(2\%)}$/AC catalyst rendered type IV isotherms, which indicated the existence of textural *meso*-pores (Supplementary Fig. S3). Indeed, 1–10 wt% La-loaded AC catalyst has higher surface area than 0.5–2 wt% W loaded $La_{5\%}$/AC (Table 1). When La loaded-on AC, it was well dispersed onto the surface of the support, increasing the surface area. This finding was in agreement with XRD result, whereby majority of $La_{1\%\text{-}10\%}$/AC exhibited smallest crystallite size (12.5–14.8 nm). Since, there was a 20–26 % pore volume reduction on pore volume of both $La_{5\%}$-$W_{0.5\%}$/AC and $La_{5\%}$-$W_{2\%}$/AC catalysts [43,44]. Hence, it is believed that lower surface area of $La_{5\%}$-$W_{0.5\%}$/AC and $La_{5\%}$-$W_{2\%}$/AC were due to partial pore blockage of small pore diameter (pore diameter: 0.53 to 0.42 nm) by small atomic radii of W (W^0: 0.014 nm; W^{6+}: 0.064 nm). Note that excess W loading (8 wt%) has the largest surface area of 980 m^2/g. The increase in surface area is likely due to the distortion of the La_0 and La_2O_3 crystal structures, caused by the integrated rich W species, which led to the development of cracks and the creation of new pores on the AC's surface. Also, the addition of W has the tendency to reduce La^0 sintering, resulting in a slighter crystallite (29.4 nm), in comparison to the other $La_{(5\%)}$-$W_{(2\%)}$/AC catalysts, and this circumstance indirectly expands the overall surface area [45,46]. The surface area play important roles in the chemicals reactions rate in general the catalyst with low surface area have a lower conversion and yield

compared to the same catalyst with the high surface area (see the screening results).

The CO uptakes of the La-W/AC catalysts are illustrated in Table 2. The greatest uptake, (128.56 mmol/g) was observed for $La_{(5\%)}$-$W_{(2\%)}$/AC catalyst. As the proportion of W rose, the CO uptake diminished, which can be attributed to the surface coverage of the catalyst support thus enhancing particle growth [47,48]. It is assumed that the W content and the dimensions of the particles are the two elements that influence CO uptake. CO uptakes were notably elevated from 29 mmol/g to approximately 39 mmol/g when the proportion of La was augmented from 1 to 10 wt%, and by 73.91 to 128.56 mmol/g when the W content was upgraded from 0.5 to 8 wt%. An additional rise in W species produced a lower exposure of active loci on the surface. When reduced metallic loading is employed, the overall tendency is for the configuration of crystals of more minute dimensions.

The data are in agreement with the findings of XRD analysis (Section 3.1), which indicated increment of catalyst's active phases with maximum 2 wt% of W loading and 5 wt% of La loading, thus generating more active loci. Additional W content appears to promote the catalyst's metallic phase distribution. Furthermore, the TPD data demonstrate that an elevation of the metal doping proportion precipitated a fall in dispersion from 33 to 27 %, whereas additional W doping caused this to rise from 33 to 88 %. Nevertheless, if W content was promoted to 8 wt%, the distribution diminished to 81 %, implying that the addition of elevated W loading suppressed active metal nanoparticle frittage. This is to some extent expected, as the decrease in crystalline dimensions are generated via the heightened metallic content, which thus diminishes CO uptake [47,48]. In relation to this phenomenon, it has been observed that an elevated phosphorous species ratio in a Ni_2P/SiO_2 catalyst enhances nickel distribution on a silica support [49].

UV–Vis diffuse reflectance spectroscopy analysis results of catalyst samples

In-depth analysis of La-W active sites for La-W/AC catalysts was further investigated via UV–Vis diffuse reflectance spectroscopy analysis (UV–Vis DRS) (Fig. 3). The presence of La-W phases demonstrates shoulder bands at approximately 249.96 and 273 nm, respectively, which reflect W^{3+}–O^{2+} or/and La^{3+}–O^{3+} charge-transfer transitions. Less robust bands evident at approximately 307 nm indicated the presence of octahedrally coordinated La^{3+} and W^{3+} species present on the AC [50]. This may be a consequence of the reduced metal oxide components and the robust engagement between La and W being suppressed by metal oxide generation; which is verified by data from H_2-TPR [47].

The distribution of active metals on the catalysts' veneer was ascertained by way of TPR analysis (Table 2). The data demonstrate that a ten-fold rise in La loading reduces the metal distribution proportion from 33.1 to 27.9 %. At lower La (1 wt%), high amount of H_2 diffusion into the matrix or the diffusion of matrix O_2 up to the surface of catalyst. In contrast, a four-fold increase of H_2 uptake for W loading 2 wt%, which enhanced the metal distribution proportion. Electronegativity associated with W (Section 2.36) is greater than that linked with La (Section 1.1). The greater dispersion is evidenced by significantly scattered constellations or as lone L and W ions that are robustly engaged with the support. A rise in W content from 2 to 8 wt% diminishes the dispersion fraction owing to saturation with loading above 2 wt% and resulted of particle aggregation. The latter was verified by XRD where high W loading enhanced the dimensions of the crystals (Table 2; Fig. 2).

The manufactured specimens' surface acidity was assayed by TPD-NH_3 (Fig. 4). In contrast to the series of $La_{(5\%)}$/AC, the catalysts loaded with W displayed a rise in the quantity of ammonia desorbed, suggesting that the W active sites rendered high acidity of the $La_{(5\%)}$/AC catalyst.

A TPD zenith within temperature ranges of 0 to 350 °C, 350 to 700 °C, and ≥ 700 °C indicates minimal, moderate or strong acidity or basicity, respectively [51]. The catalysts exhibited a range of peaks at diverse temperatures within the TPD-NH_3 spectra. Desorbed peaks observed at 137 and 640 °C reflected low and moderate acid sites of the monometallic catalysts ($La_{(5\%)}$/AC) (Fig. 4). In contrast, TPD- NH_3 data indicated that La-W/AC catalyst with addition of W active sites promote the acidity of catalyst with low (200 °C) and strong acid strength (896 °C) of active sites [52].

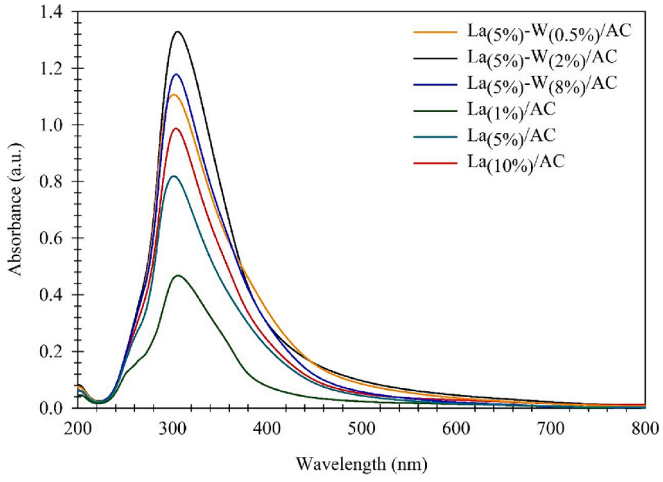

Fig. 4. UV vis Analysis of the supported catalyst.

Table 2
Temperature programmed desorption (TPD), reduction (TPR) and pulse chemisorption (TPD CO, CO_2 NH_3) of La-W/AC catalyst.

Catalysts	Nominal loading wt%		Actual loading wt % (±0.9 %)[b]		Chemisorption				FTIR-pyridine	
					TPD-CO	TPR	TPD-NH_3			
	La	W	La	W	CO uptake (mmol/g)[a]	% of metal dispersion	Desorption temperature[a] (°C)	Amount of NH_3 adsorbed[a] (μmol/g) ± (4 %)	Lewis	Brønsted
$La_{(1\%)}$/AC	1	–	0.8	–	32.54	33.1	137,635	458.10	108.66	284.66
$La_{(5\%)}$/AC	5	–	5.3	–	39.90	31.4	139/637	971.62	261.56	569.24
$La_{(10\%)}$/AC	10	–	10.6	–	29.64	27.9	134/640	729.38	219.68	401.45
$La_{(5\%)}$-$W_{(0.5\%)}$/AC	5	0.5	4.8	0.4	73.91	88.6	140/896	3465.44	517.04	2489.29
$La_{(5\%)}$-$W_{(2\%)}$/AC	5	5	5.3	1.8	128.56	81.0	145/940	13319.16	2306.87	9214.62
$La_{(5\%)}$-$W_{(8\%)}$/AC	5	8	5.1	8.6	116.73	58.2	898	7910.47	357.55	6590.29

[a] Determined by integrating the area of CO/NH_3/CO_2-TPD chemisorption peaks.

Generally, the TPD-NH_3 parameters of the catalysts indicate a vibrant engagement, between the AC support and the two metals. The most significant variation identified, between the $La_{(5\%)}$/AC and the $La_{(5\%)}$-$W_{(2\%)}$/AC catalysts, has to do with differences in acidity. The addition of W to $La_{(5\%)}$/AC led to an increase in acidity, as each acid comes with $6H^+$ medium loci that are exchanged with a single W^{+6} ion to sustain charge equilibrium, which is $6H^+/W^{+6} = 1$ [32]. This will prompt the introduction of a de novo NH_3 desorption zenith, specifically the robust acid loci on the $La_{(5\%)}$-$W_{(2\%)}$/AC catalyst. Moreover, the marginal variations observed in the RT locations, and the potency of the medium and concentrated acid loci in the spectra following W loading at 2 wt%, indicates that the quantity and strength of the acid loci were preserved, thus maintaining the reliability of the catalyst, with regards to the standard DO reaction of WSPO. The enhancement of the acid loci density through W-doping is an indication that the acidity level of W is higher than that of $La_{(5\%)}$/AC. The acidity profile of the prepared catalyst as flow $La_{(5\%)}$-$W_{(2\%)}$/AC > $La_{(5\%)}$-$W_{(8\%)}$/AC > $La_{(5\%)}$-$W_{(0.5\%)}$/AC > $La_{(5\%)}$/AC > $La_{(10\%)}$/AC > $La_{(1\%)}$/AC.

Pyridine FTIR analysis of La-W/AC catalysts was conducted to evaluate the concentrations of the surface acid loci of the catalyst. Following evacuation at 300 °C, the FTIR spectra of catalysts including chemisorbed pyridine were estimated (Fig. 5). A zenith observed at 1527 cm^{-1} represented pyridine ions that interact with the catalyst's Brønsted acid loci (BPy). FTIR peaks observed at 1468 and 1489 cm^{-1} reflected adsorbed pyridine on Lewis's acid loci (LPy). Following addition of W loading, no reduction in band strengths linked with either BPy or LPy on the surface was evident. When judged against the de novo $La_{(5\%)}$/AC, the La-W/AC catalysts displayed more marked peak strengths at 1412 and 1615 cm^{-1}, which denoted real LPy loci, i.e. under synchronised La^{3+} or surface AC, and W^{6+} cations [36].

The modest rise in strengths at the latter two wavelengths was potentially the result of spectral imbrication of LPy on the catalyst veneer and available W ions close to the AC surface following W loading. Pyridine FTIR demonstrated that a higher proportion of the acid loci on the extrinsic La-W/AC catalyst surface was conserved, suggesting the synergistic effect between the bimetallic interaction of La-W.

Notably, was that the AC's pore radius had a typical wavelength of 15.332 Å. Given that pyridine has a dimension of 5.7 Å and that its spatial restrictions are notably higher than for NH_3 (3.3 Å), the pyridine may not be able to penetrate the acid loci within the pores of the AC [37]. Thus, pyridine FTIR essentially identifies the external acid surface loci and a fraction of the intrinsic sites that lie close to its exterior. Nevertheless, since NH_3 is a small compound, both AC intrinsic and extrinsic surface loci are available to it. The rise in NH_3 vapour desorption during TPD-NH_3 following W loading is a distinctive trait of the presence of W on internal LPy.

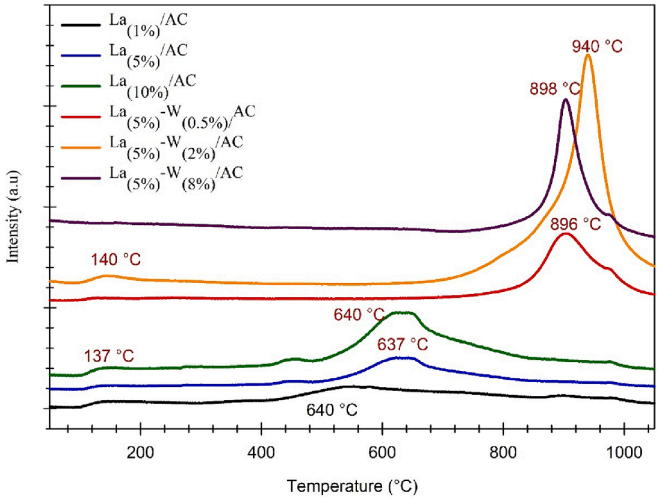

Fig. 5. TPD-NH_3 analysis for the AC supported catalyst.

FTIR pyridine adsorption provides insights into the nature and strength of acid sites on the catalyst surface. Moreover, the FTIR pyridine is a qualitative analysis compared to the TPD-NH_3 the results were tabulated in Table 2. The acid values from FTIR- pyridine were in line with the TPD-NH_3 analysis. The FTIR pyridine slows less total acid value by ± 14 % from the TPD-NH_3.

WSPO catalytic DO reaction

The DO of WSPO, catalysed by $La_{(5\%)}$/AC and La-W/AC catalysts, delivers a wide distribution of products including liquid *n*-alkanes and alkene (*n*-C7 – *n*-C20), oxygenated intermediate substances including alcohol, aldehyde and ketones, as well as vaporised CO and CO_2. The DO pathway proposal (Scheme 2) is based on product distribution research, as well as the results derived through previous studies. The WSPO-CO_2 pathway produces *n*-C_{17}, O_2 is removed in the form of H_2O, and/or alcohol is generated by way of the –CO_2/–CO pathway of WSPO, and the oxygenated intermediates, with the O_2 eradicated as CO.

Amongst the prepared catalysts with either single metal or bimetallic-based catalysts (i.e. and La-W/AC), the $La_{(5\%)}$/AC and $La_{(5\%)}$-$W_{(2\%)}$/AC offered the efficient of WSPO conversion to *n*-C_{17} HC. The catalytic activity of La-W/AC catalyst was affected predominantly by the surface density of La and W, as well as the acidity-basicity of the catalyst. Besides, results indicated that the TOF of WSPO was increased as the increment of La-W loading (Fig. 6). Fig. 6 and Fig. S5 shows increasing in the acidity lead to increase in the green diesel yield and n-C17 selectivity. High deoxygenation activity by $La_{(5\%)}$-$W_{(2\%)}$/AC is highly parallel with largest weak + medium acid sites concentration and to the nature of W and La itself that tends to yield hydrocarbon rich output mainly via cracking pathways. High yield of fuel-like hydrocarbon by mixed metal oxide supported AC catalysed deoxygenation suggested that combination of strong oxygen affinity metals (La and W) are beneficial for weakening the C-O single bonds and ultimately ensuring the removal of oxygenates species. The catalyst deoxygenation of the prepared catalysts with the trend of $La_{(5\%)}$-$W_{(2\%)}$/AC > $La_{(5\%)}$-$W_{(8\%)}$/AC > $La_{(5\%)}$-$W_{(0.5\%)}$/AC > $La_{(5\%)}$/AC > $La_{(10\%)}$/AC > $La_{(1\%)}$/AC > $W_{(8\%)}$/AC > $W_{(2\%)}$/AC > $W_{(0.5\%)}$/AC > AC which is in line with he TPD-NH_3 and FTIR-pyridine results.

Optimisation study of the reaction parameters

Pre-screening studies indicated that the bimetallic $La_{(5\%)}$-$W_{(2\%)}$/AC catalyst showed best DO efficiency for WSPO. Therefore, this catalyst was selected for optimisation study to assess the relevant responses (e.g WSPO conversion, product selectivity, TOF) based on the reaction parameters, i.e. RT, CL, and reaction time (Rt).

CL effect

Fig. 7 depicts the influence of CL on WSPO conversion and product selectivity, based on C number. The DO reaction was maintained for 30 min, under a RT of 250°, and a stirring rate of 500 rpm, within an inert N_2 atmosphere. The influence of CL, from 0.1 wt% to 3 wt%, was then assessed. According to the findings derived, while the DO performance and *n*-C_{17} selectivity were both elevated over a CL range of 0.1 to 0.5 wt %, the performance declined with catalyst loads > 0.5 wt%. WSPO conversion and product selectivity for *n*-C_{17} were observed to be outstanding at 67.40 and 67.81 respectively, with a catalyst loading of 0.5 wt%. An increase in the catalyst load led to a climb in TOF from 0.066 to 0.0153 s^{-1}, which can be attributed to the rise in the active loci count. On the other hand, a dip in the DO performance and *n*-C_{17} selectivity, with catalyst loads above 0.5 wt%, is an indication of overloading. Catalyst overloading encourages the occurrence of secondary and concurrent side reactions, which is attributed to the excess active loci for non-beneficial pathways [46]. As such, in terms of efficiency and cost-effectiveness, the CL of 0.5 wt% is considered ideal for the DO of

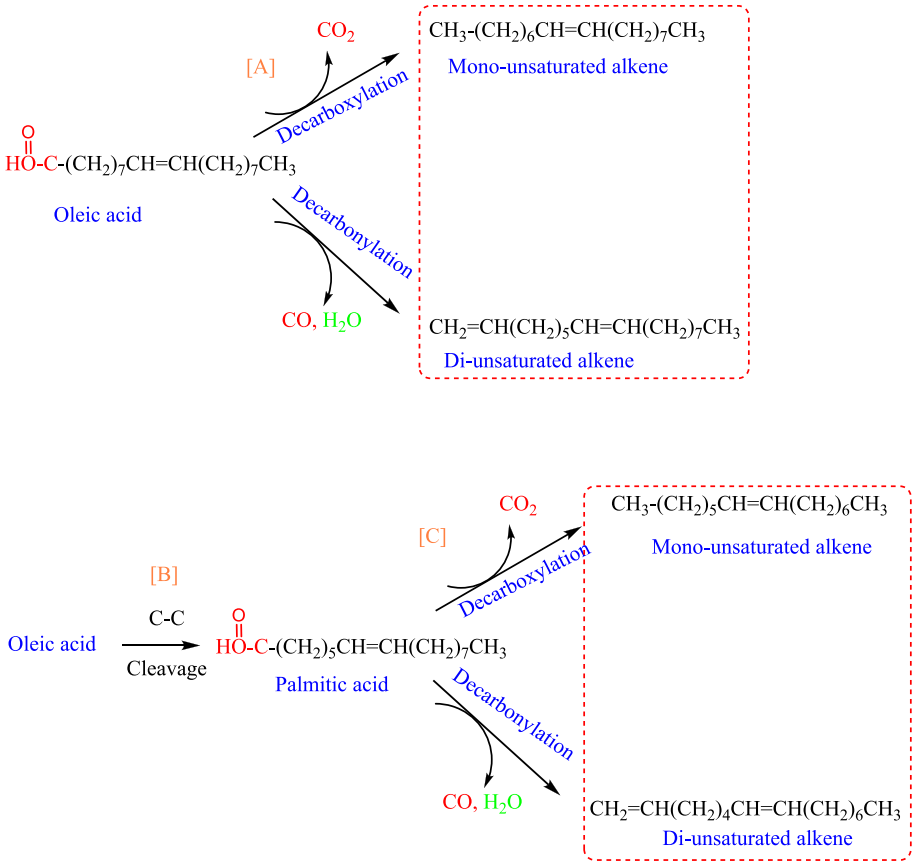

Scheme 2. DO reaction mechanism of SPO.

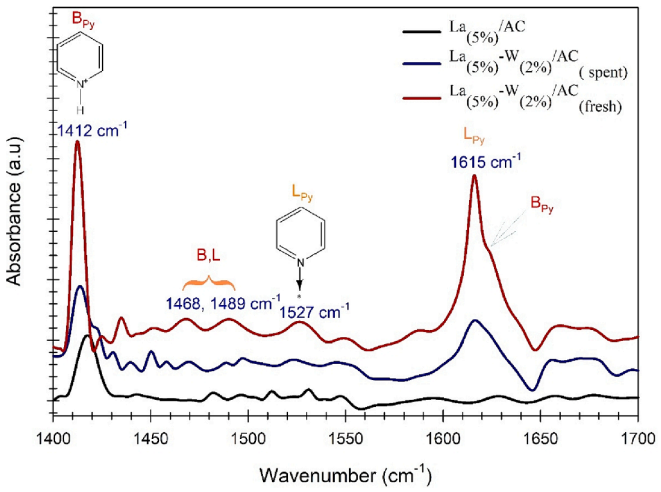

Fig. 6. FTIR pyridine spectra of the supported catalyst.

WSPO.

Rt influence

The assessment results for the effect of Rt on the DO of WSPO are exhibited in Fig. 7c and d. DO was carried out within a range of Rts, (30 min to 240 min) at a RT of 230 °C. CL was at 0.5 wt%, the stirring rate was set at 500 rpm, and the reaction was performed under an inert atmosphere.

Predictably, hydrocarbon transformation escalated with an extension of the Rt, as depicted in Fig. 7c and d. Within the initial 30 to 60 min, both hydrocarbon transformation and *n*-C_{17} selectivity were significantly enhanced from 34 % to 89 %, and from 79 % to 94 % respectively. This suggests that extended Rts, can serve to elevate the DO performance via deCOx pathways, by raising the capacity of the compounds involved, to react with the catalyst's surface. Upon breaching 60 min Rt, however, *n*-C_{17} selectivity was reduced to 77 %. This is attributable to the additional fracturing of the product, into segments of lesser weights. This development facilitates the generation of vapourised materials, and the deactivation of the active loci on the catalyst, by way of a side reaction [53]. Furthermore, a decrease in TOF was observed from 8.22 x 10^{-3} s^{-1} to 2.70 x 10^{-3} s^{-1}. Thus, in terms of HC transformation and *n*-C_{17} selectivity, optimum 60 min of Rt was selected to be extremely efficacious for the best DO performance through the deCOx pathways.

RT influence

The effects of RT, within the range of 230° and 300°, with regards to the DO of WSPO, was investigated (Fig. 7e and f). The reaction was initiated with a CL of 0.5 wt%, and a 60-minute stirring period at 500 rpm, within an inert environment. Clearly, the increase in RT from 230 °C to 250 °C, significantly enhanced the WSPO conversion from 85.35 % to 98.50 %. This conversion level dipped marginally, when the RT was elevated to 275 °C. This pattern was repeated for the *n*-C_{17} selectivity, where the peak occurred at a RT of 250 °C, and at 300 °C, the selectivity level fell to 61 %.

High reaction rate of DO at RT of 250 °C promote the reactivity of deCOX indicated the well dispersed of La-W/AC particles in the fluid state, which simultaneously enhanced the efficiency of mass transfer between the reaction components [54]. Nevertheless, further increased of RT above 250 °C caused a reduction in DO performance. It can be postulated that the extreme RTs could generate additional cracking within the pathways, thus generating vapour products and lessening the transformation of the fluid components [55]. The optimum reaction

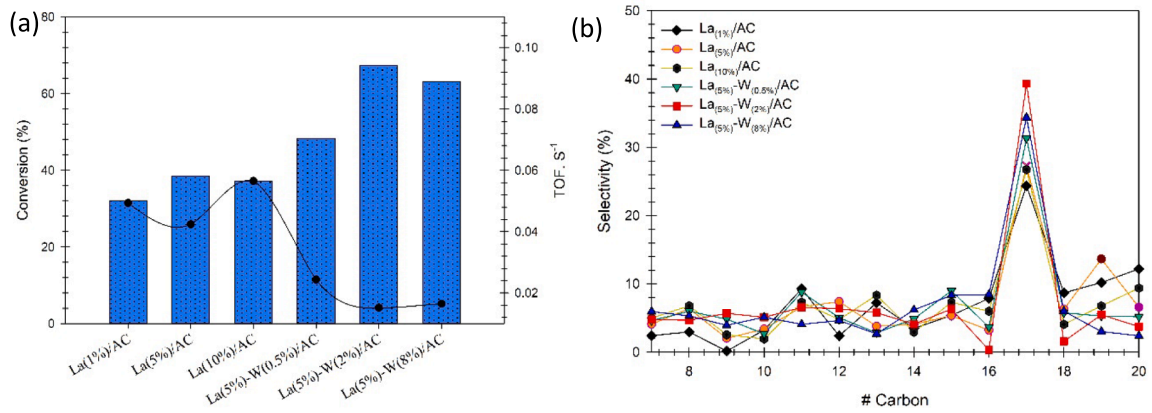

Fig. 7. DO reaction screening of WSPO (a) conversion and TOF and (b) HC selectivity over supported catalyst. Pressure 1 ATM, stirring speed 500 rpm, and reaction time 30 min.

conditions of the WSPO over the prepared catalyst were catalyst loading of 0.5, time of 60 min and reaction temputer of 250 °C.

The TOF was additionally augmented by a rise in RT from 230 to 300 °C as a consequence of greater active loci exposure. The superior RT produced a HC transformation of 98.50 %, with selectivity for *n*-C_{17} consistuents of 93 %. The present study suggest that the optimum outcome can be attained with CL of 0.5 wt%, a RT of 250 °C, a Rt of 60 min under inert conditions. Compered to other published work reserchers, used H_2 gas at high temperatures and high pressuer inorder to hydrogenated the C = C on the other hand the catalyst reqierd high temperature to activated the carbon duble bon carbon such as the sutedu reported by Srifa et al., the reaction temperature of 420 °Cwith H_2 pressure 80 bar [56].

Assessment of the stability and reusability of the catalyst used for the DO of WSPO

The assessment of stability and reusability features of bimetallic $La_{(5\%)}$-$W_{(2\%)}$/AC was conducted by using the optimum parameters for the DO process, i.e. CL of 0.5 wt%, a RT of 250 °C, a Rt of 60 min, and inert conditions. Once the DO reaction was concluded, the spent catalyst was salvaged through simple and repetitive cleaning with hexane solution, subsequently being reused with the same reaction conditions. The reusabillity data indicated an consistent catalytic DO acticity for up to three reaction repetitions (Fig. 8), while gradually reduction of WSPO conversion from 98.50 to 87.36 % for eight runs of studies. The slight reduction of catalyst reactivity was due to the leached of active W^{3+} and La^{3+} ion into the reaction medium, which was further confirmed by ICP-AES analysis. The ICP-AES data (Fig. 8) showed the slight increment of W^{3+} and La^{3} concentration (from 1st to 8th run, which reflected low amount active metal leaching occurred throughout the reusability study. In general, it was estimated that the metal leaching in the fluid phase product comprised 1.8 ppm per cycle from the 1st to 8th runs; these concentrations are well below the maximum level of contamination content, 24 ppm, dictated by EN 12662 Standard Specification for Diesel Fuel Oils. These data therefore verified that the La-W/AC catalyst exhibits robust resistance to leaching and has outstanding structural integrity. The meatal leaching has a noticeable reduction in the green diesel conversion, one of the important types of catalyst deactivation is by metal leaching. metal leaching lead to reduce in the active sites of the catalyst and reduce the acidity/ basicity of the catalyst which will affect directly the reaction rate, conversion and selectivity.

Evaluation of catalyst deactivation

In addition to the reusability tests, it is crucial to study the catalyst deactivation mechanism, aiming to identify the generated C products, as well as quantify their amounts, and understand their correlation with the structural stability during WSPO DO reaction. Therefore, the catalyst deactivation was investigated via in-situ operando and ex-situ analysis. X-Ray diffraction analyses were done after eight runs of reaction for the $La_{(5\%)}$-$W_{(2\%)}$/AC catalyst. The XRD results show a broad patten at 2θ: 25.11° attributed to the formation of coke (Fig. 9) [57]. According to the XRD analysis results, the reactivated catalysts portray comparable patterns, with insignificant alterations in crystallinity. This findings suggesting that the $La_{(5\%)}$-$W_{(2\%)}$/AC catalyst is highly stable, which was in agreement with ICP-AES study with negligible of low La-W leaching content (Fig. 8).

Fig. 9b depicts TGA profiles of the fresh and the spent $La_{(5\%)}$-$W_{(2\%)}$/AC catalysts. The fresh $La_{(5\%)}$-$W_{(2\%)}$/AC catalyst showed approximately 71.63 % at 352 °C of the weight loss, which was attributed from oxidation of C species under O_2 condition. However, the weight change of spent $La_{(5\%)}$-$W_{(2\%)}$/AC after the reaction (eight runs) showed two degradation stages at 223 to 343 °C and 361 to 469 °C.

The first step was due to the oxidation of soft coke which was deposit during the DO reaction, while the second weight loss was ascribed to oxy-carbonate or strongly adsorbed CO_2 [58,59], and it was confirmed by the mass spectrometer analysis about the releasing of the CO_2 and CO during catalyst heating under O_2 atmosphere. Referring the mass spectroscopy results the CO and CO_2 are released by the degradation of the coke formatted over the catalyst surface this were confirmed by the XRD results of the spent catalyst Fig. 9. The reduction of the WSPO conversion is due to the covered the active site by the coke formation which will prevent the FFA molecule's from attached to the active site. The target deoxygenation products of WSPO conversion are hydrocarbons, so it's critical to comprehend the reaction pathways that lead to the formation of these products as well as those that result in undesired condensation (heavy) products. These pathways can deactivate catalysts by oligomerizing unsaturated hydrocarbons and heavy compounds to coke, which blocks the catalyst's active site and reduce selectivity.

Coke formation mechanism of $La_{(5\%)}$-$W_{(2\%)}$/AC catalysed DO of palmitic acid

In order to conduct a deeper analysis and elucidate the coke formation mechanism of $La_{(5\%)}$-$W_{(2\%)}$/AC, in situ XPS and UV-Raman analysis was further conducted. Palmitic acid was selected as the model compound of WSPO due to its high composition withing the feedstock. To monitor the surface changes of the $La_{(5\%)}$-$W_{(2\%)}$/AC catalyst during the DO reaction of palmitic acid, in situ XPS analysis helps to determine the amount of deposited coke and the element oxidation phase changed, where data were collected every 240 min for 1440 min (Fig. 11 and Supplementary Figs. S2 and S3). Fig. 10a and S2 show the evolution of C1s during the reaction. The measurement of all elements is initially calibrated by the binding energy of the C1s peak (284.8 eV). Following 240 min of reaction, the entire XPS spectrum

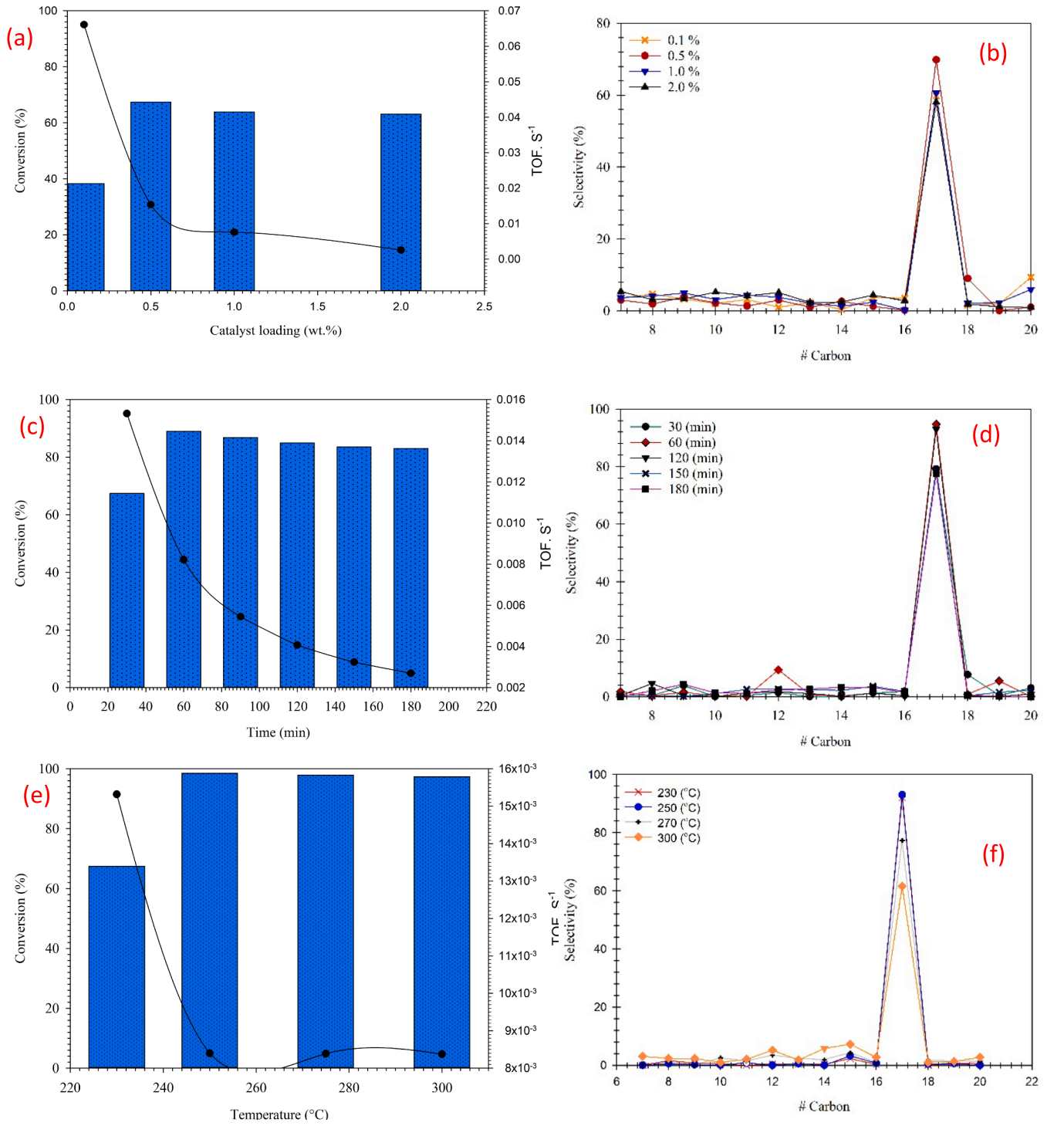

Fig. 8. Optimization investigation on the effect of catalyst amount of WSPO (a-b) DO on the reactions of $La_{(5\%)}$-$W_{(2\%)}$/AC; reaction conditions: 230 °C, 30 min (b-c), DO reactions of $La_{(5\%)}$-$W_{(2\%)}$/AC catalyst influenced by Rt; reaction conditions: 0.5 wt% CL, 230 °C (e-f), DO reactions of $La_{(5\%)}$-$W_{(2\%)}$/AC catalyst influenced by RT; reaction conditions: 0.5 wt% CL, 60 min at 500 rpm under N_2 flow.

experienced a shift of 0.1 − 0.3 eV, to a loftier BE. As mentioned previously, this shift is a consequence of the bending of the band in the C-C, C = O, C-O-C and C-M or M−C−M*, which is attributed to the electronic interaction with the deposited coke [53,54].

As the Rt extended from 240 to 1440 min, the C1s core was altered by ~0.1 eV to lower BE. This is an indication that the quantity of coke increased, while the original $C1s_{serf1}$, and the $C1s_{serf1}$ corresponding to the AC support, decreased in magnitude and peak intensity. It is likely that this latest feature at lower BE, stems from the formation of nanoscale C at the interface. However, the full width at half-maximum (FWHM) of the reduced peaks, also increased marginally with coke deposition. This can be attributed to the presence of convoluted peaks, deriving from the multiple oxidation of the active element.

On the other hand, Fig. 10b show the peak changed for the La3d, the XPS show a shifting to lower binding energy ~ 0.2–0.4 eV that due to the interface to the C and the O_2 atom. However, the fact that La is highly reactive which lead to easily reactive to the O_2 atom from the CO_2 (from the side product of the decarboxylation reaction) to form surface

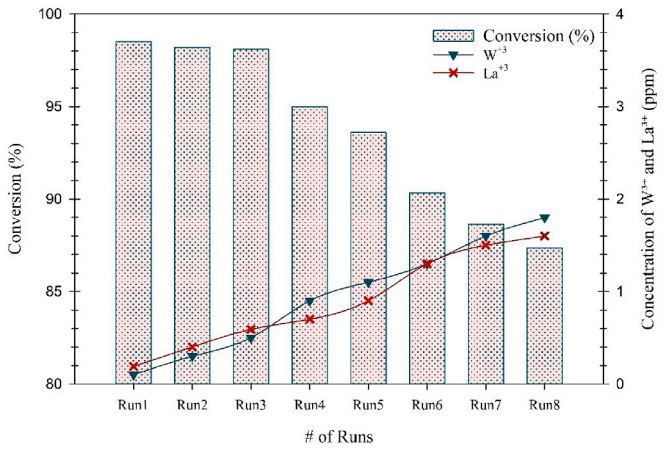

Fig. 9. Reusability of $La_{(5\%)}$-$W_{(2\%)}$/AC catalyst at the optimum conditions: 0.5 wt% CL, 60 min, RT 250 °C, and 500 rpm under N_2 flow.

carbonates. We noticed that the La peak show increasing of intensity and shifted to lower binding energy for the $La(OH)_3$ due to the hydrolysation of La with water from the side product of the decarbonylation pathway ($CO + H_2O$). By the time increasing the peak intensity is increased this indicated that the amount of the $La(OH)_3$ increasing. However, we observed that the catalyst is best matched with symmetric peak shapes, while transition metals are mostly matching with asymmetric peak shapes. This may be an indication that a minor quantity of La and W with intermediate oxidation states is also present. This situation could be attributed to the partial reaction of the CO, H_2O, and CO_2, with some of the La and W (Fig. 12).

Fig. 11c show the effect of the Rt on the W4f core level. The peaks were shifted to lower binding energy indication the increase of the amount of the specific oxidation status of the W through prolong Rt. We observed that the increase in Rt, led to the appearance of new peaks ($WC_{5p3/2}$ and $W^{6+}_{4f5/3}$), and the decrease in O_2 vacancy. This situation brings about an increase in the coordination number of the metal (W), and the merging of the O_2 atom with the metal atom, to form an M−O bond (Figs. S6 and S7) (Fig. 13).

The operando UV-Raman of $La_{(5\%)}$-$W_{(2\%)}$/AC catalyst during DO of WSPO under the optimum condition was shown in Fig. 11a. During the 360 min of RT, distinct alterations in the spectroscopic features were observed. The spectrum, of the bare La-W/AC, is devoid of any significant feature in the range of interest. However, after 360 min, a single weak band, attributable to framework modes at 1542 cm^{-1}, was transferred to a higher wavelength of 1560 cm^{-1}. Upon HC dosage, the intensity of the peak, with its maximum at 1635 cm^{-1} grew rapidly during the initial 60 min. The same band moves by 5–10 cm-1 throughout the early phases. Through n-C15, the bands at 1560 cm-1 and 1415 cm-1 rise in tandem and with comparable strength. Meanwhile, two delicate bands appear with n-C15 at roughly 1600 cm-1 and 1670 cm-1, albeit at a considerably slower rate and to a little extent. The only band that has lost strength is the one at 1370 cm-1, which used to be plainly opposed to the band at 1635 cm-1. Notably, increasing n-C15 causes a 5 cm-1 blue shift in the 1370 cm-1 band.

According to the UV-Raman analysis, the collaborative intensity tendency indicates that the bands at 1635 cm-1, 1560 cm-1, and 1415 cm-1 are associated with chemical species classified as alkenes. These findings are confirmed by the known preservation of n-Cn + alkenes inside the pore of AC, which is attributable to the fact that the smaller pore size of AC prevents alkene out-diffusion from the framework. The 1600 cm-1 wavelength is assigned to the G band of amorphous C, whereas the D band is restricted due to the use of UV stimulation during measurement [60,61]. Because the high frequency shoulder, at 1670 cm-1, is inside the carbonyl stretching area, it can enable the presence of oxygenated compounds (unreacted from the palmitic acid). However, it should be noted that many branched olefins can emit signals at this frequency. Finally, the 1370 cm-1 frequency range is prevalent for polycyclic aromatic HCs signatures (verified by GC–MS analysis) [62]. Polysubstituted aromatic HCs (1380 cm-1), polysubstituted cyclohexenes (1400 cm-1), and polycyclic aromatic HCs are examples of small polycyclic aromatic HCs with strong properties that are close to this frequency (1350 cm-1) [63]. However, none of these characteristics fully work with this band. The signal is fairly broad (FWMH of around 35 cm-1, twice that of pure polycyclic aromatic HCs), which is significant since it implies that numerous molecules' properties overlap.

The online MS signals offer information on the catalyst's chemical behaviours during the process, as illustrated in Fig. 11b. The n-C_{17} and n-C_{15} HCs exhibit the most unpredictable response patterns in this regard. There are no discernible products in the gas phase, and the reaction's ion current slows very quickly at first. When signals from the products start to appear, the n-C_{17} and n-C_{15} signals quickly increase. After that, they exhibit a very steep slope and a slow rate of growth until the experiment is over. The cause of this atypical progression linked to the n-C_{17} and n-C_{15} signals is ascribed to the physisorption of n-C_{17} and n-C_{15} at the reactor cell's cool glass sections, as well as the concurrent accumulation of the HC pool within the catalyst's pores. A larger amount of vapour travels through the whole reactor for MS measurement because the n-C_{17} and n-C_{15} vapours completely saturate all of the glass sections. This explains the previously noted brief spike in signals. On the other hand, pertinent literature refers to the induction time—which is typically between 10 and 20 min—prior to product detection as the

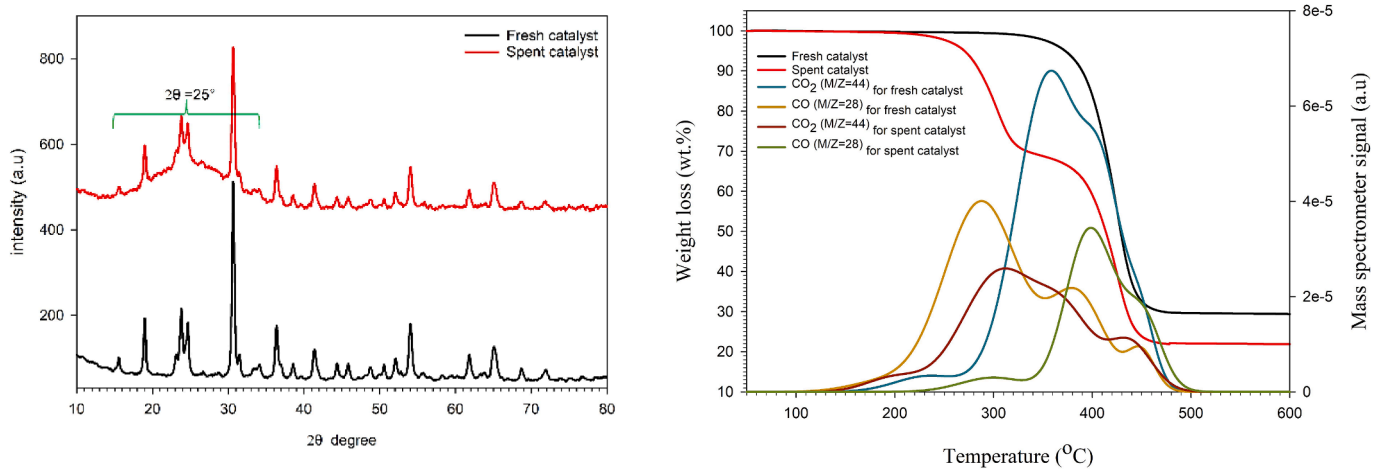

Fig. 10. (a) XRD results of $La_{(5\%)}$-$W_{(2\%)}$/AC catalyst after recycle and (b) TGA-MS for fresh and spent catalyst indicating CO_2 and CO gas release from the catalyst.

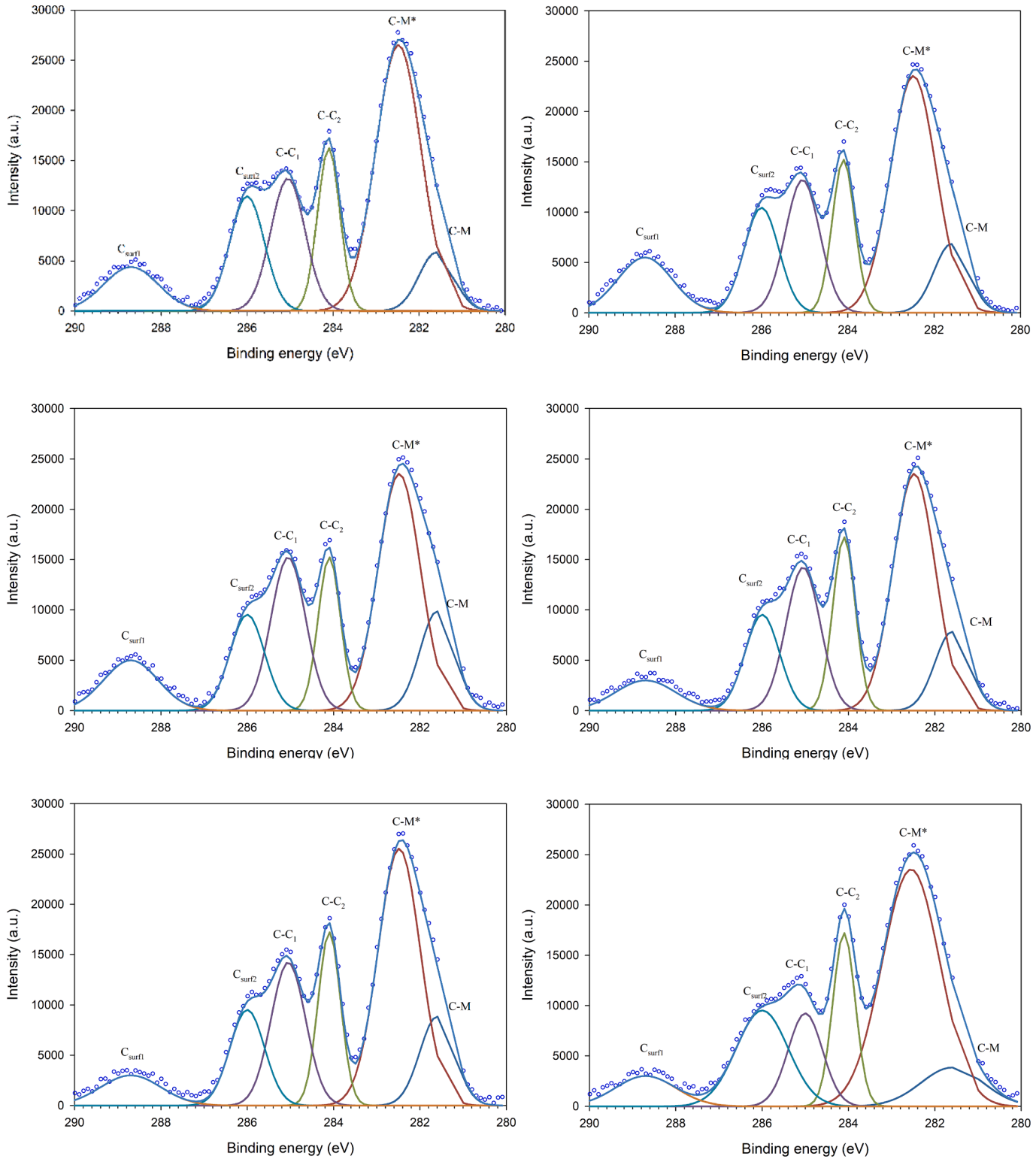

Fig. 11. In situ XPS analysis for C1s with different Rt from 30 to 1440 min of $La_{(5\%)}$-$W_{(2\%)}$/AC catalyst.

decisive determinant for the principal size of the AC particles. A prolonged DO reaction causes a progressive decline in catalyst activity. This gradual deactivation activity has been discussed during previous studies. No aromatics were detected all through the experiment, which can be attributed to selectivity imposed by the small-pore topology of AC.

During the early stages of DO, the dominating spectral features derive from palmitic acid (the AC pool) and a portion of amorphous C. This portion of amorphous C, which was probably developed during the initial reaction phase by active sites assembled on the external surface of the catalyst's particles, is quickly deactivated to curtail the further extension of the carbonaceous phase. Indeed, its Raman signals (specifically the G band at 1600 cm^{-1}), increased only marginally during DO reaction. Although the amorphous C quantity at this stage is depleted, its low penetration depth allows for the investigation of near-surface species, by way of UV-Raman. During the initial observation of the products

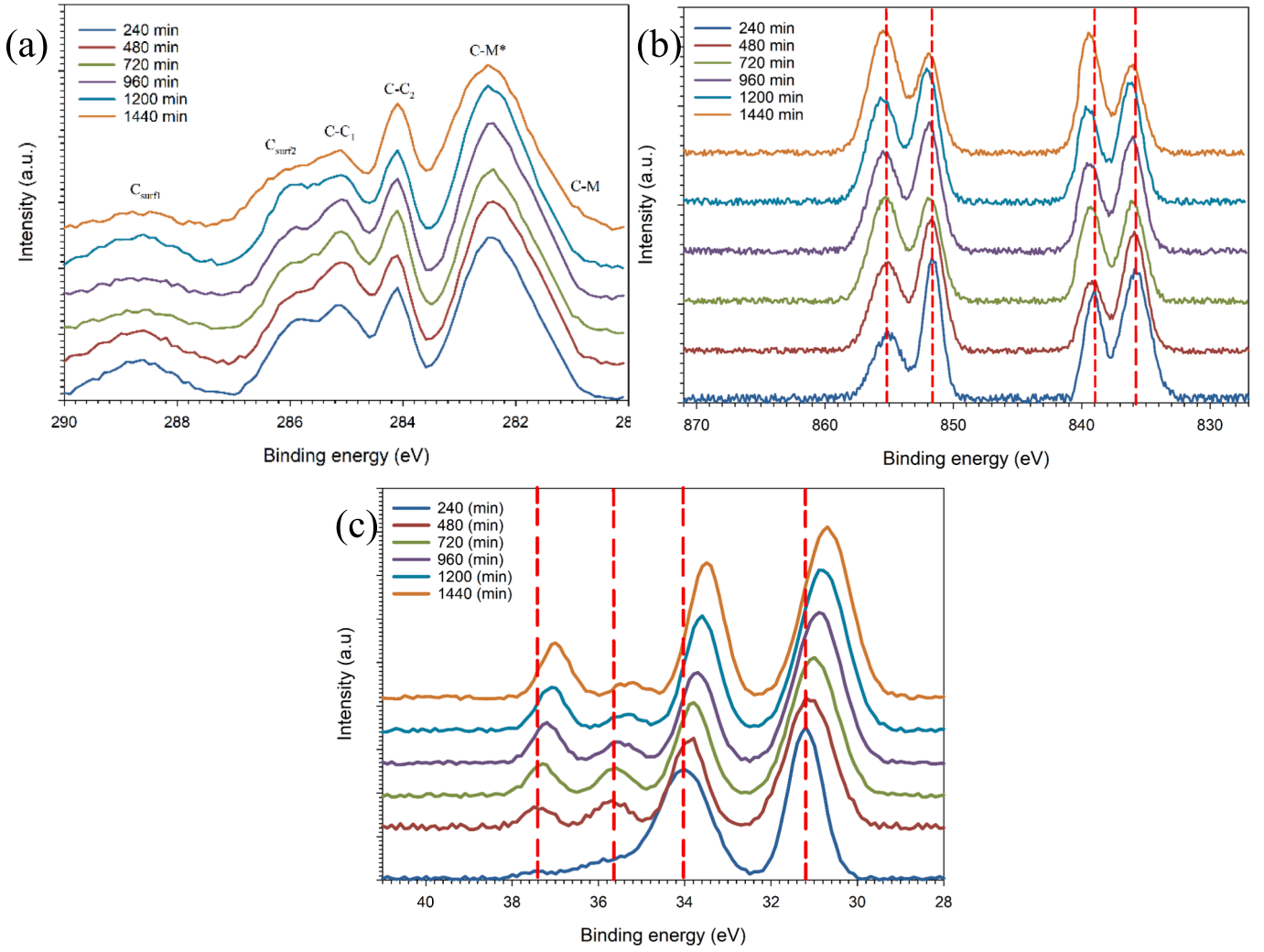

Fig. 12. In situ XPS analysis for $La_{(5\%)}$-$W_{(2\%)}$/AC catalyst. (a) C1s, (b) La 3d and (c) W4f with different Rt from 240 to 1440 min at the optimum reaction conditions.

by MS, specific HCs (1370 cm^{-1} and 1625 cm^{-1}) decrease in intensity, and signals associated with alkenes (1635 cm^{-1}, 1560 cm^{-1} and 1415 cm^{-1}) begin to climb. Eventually, a diminished quantity of carbonyl-containing species/branched alkenes is perceived at the closing DO of palmitic acid. The observed MS and Raman signals evolution indicate that polycyclic aromatic HCs make up a part of the HCs pool. Polycyclic aromatic HCs, which are highly abundant at the initial reaction phase, then begin to decrease in quantity as the reaction progresses, implying their transformation into other chemical species, most likely into larger polycyclic aromatic HCs (which, due to their reduced resonance, are more difficult to detect than smaller polycyclic aromatic HCs). The slight increase in features, relating to a prolonged C phase (the regular G band signal at 1600 cm^{-1}), further verifies the conversion of polycyclic aromatic HCs into other molecular species, instead of into extended coke. This situation is attributed to the established incapacity of polycyclic aromatic HCs for diffusion through the small pores of AC to arrive at the external surface (the amorphous C formation region). Their inability for diffusion, out of the framework, hinders their capacity for further reaction, which could render them a deactivating force in AC. This combination of aromatics and alkenes, leading to deactivation in AC, is in agreement with the findings documented by Rojo-Gama et al. [64], and Hereijgers et al. [65].

Conclusion

The present work reported the synthesis and catalytic study of bimetallic La-W/AC catalyst $La_{(5\%)}$-$W_{(2\%)}$/AC for catalytic DO of WSPO to HC-type green diesel. The WSPO was practically converted with HC yield of > 98 % under optimum parameters (CL, 0.5 wt%; Rt, 60 min; RT, 275 °C). The $La_{(5\%)}$-$W_{(2\%)}$/AC catalyst can be salvaged from the ensuing admixture and recycled on numerous occasions after heating to high RT without any significant alteration in the harvested HC fraction. The predominant fluid phase products can be separated in a straightforward manner utilising a cold trap.

Despite the fact that the solid catalyst employed in this study has a tendency to offer a large product harvest in mild reaction circumstances, heterogeneous catalysts demonstrated unmatched benefits compared to their more conventional and uniform counterparts in relation to reusability and apparatus damage. Thus, further research will remain concentrated on the design of innovative and environmentally friendly catalysts which exhibit superior performance for the generation of green diesel.

CRediT authorship contribution statement

A. Afiqah-Idrus: Writing – original draft, Project administration, Data curation. **G. Abdulkareem-Alsultan:** . **N. Asikin-Mijan:** Writing – review & editing, Writing – original draft, Formal analysis, Data curation. **Maadh Fawzi Nassar:** Validation. **Lee Voon:** Writing – review & editing. **Siow Hwa Teo:** Software. **Tonni Agustiono Kurniawan:** Software, Project administration, Conceptualization. **Nur Athirah Adzahar:** Formal analysis. **M. Surahim:** . **Siti Zulaika Razali:** Data

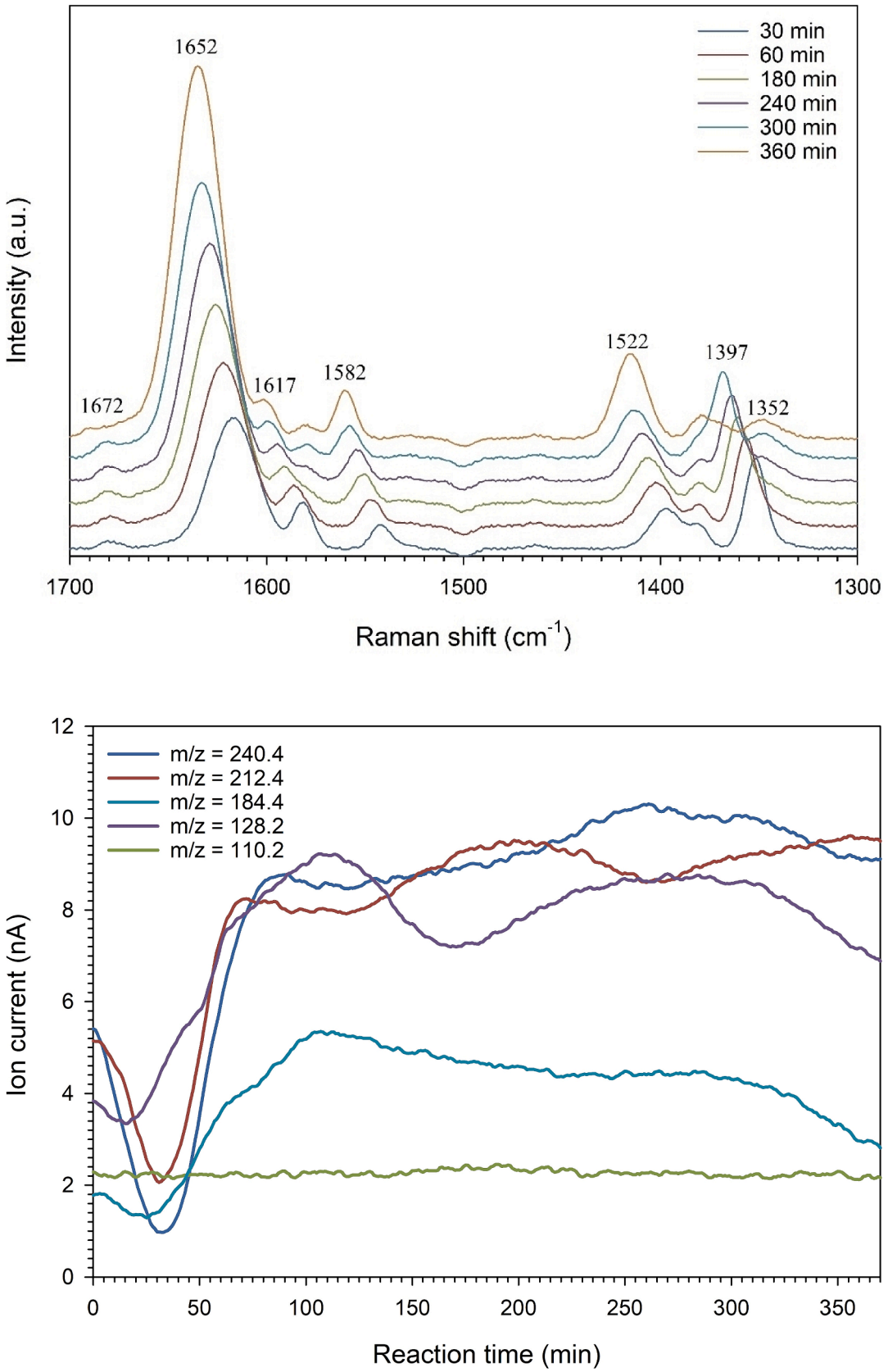

Fig. 13. a) UV-Raman spectra of $La_{(5\%)}$-$W_{(2\%)}$/AC along 360 min of DO reaction (250 °C, with 1 $g.cat^{-1}h^{-1}$ of palmitic acid to catalyst) collected every 30 min using Linkam CCR1000 reactor cell. b) Online MS charts for selected reagents/products: n-heptadecane m/z = 240.5 (n-C_{17}), n-pentadecane m/z = 212.42 (n-C_{15}), n-nonane m/z = 128.2 (n-C_9), n-tridecane m/z = 184.37 (n-C_{13}), and trimethylcyclopentene m/z = 110.20 (n-C_8).

curation, Conceptualization. **Aminul Islam:** Validation, Software, Methodology. **Robiah Yunus:** Resources, Project administration. **Noor Alomari:** Writing – original draft, Visualization. **Yun Hin Taufiq-Yap:** Supervision, Funding acquisition.

Declaration of competing interest

The authors declare that they have no known competing financial interests or personal relationships that could have appeared to influence the work reported in this paper.

Data availability

No data was used for the research described in the article.

Acknowledgement

The authors acknowledge the financial support from Ministry of Higher Education Malaysia for Fundamental Research Grant Scheme (FRGS/1/2023/STG04/UKM/02/6).

References

[1] Al-Jaberi SHH, Rashid U, Al-Doghachi FAJ, Abdulkareem-Alsultan G, Taufiq-Yap YH. Energy Convers Manag 2017;139:166–74.
[2] Alsultan A, Mijan A, Yap T. Mater Sci Forum 2016;840:348–52.
[3] Kamaruzaman MF, Taufiq-Yap YH, Derawi D. Biomass Bioenergy 2020;134:105476.
[4] Correia LM, de Sousa Campelo N, Novaes DS, Cavalcante CL, Cecilia JA, Rodríguez-Castellón E, et al. Chem Eng J 2015;269:35–43.
[5] Hayyan A, Alam MZ, Mirghani MES, Kabbashi NA, Hakimi NINM, Siran YM, et al. Fuel Process Technol 2011;92:920–4.
[6] Dujjanutat P, Muanruksa P, Kaewkannetra P. MethodsX 2020;7.
[7] Abdullah NH, Hasan SH, Yusoff NRM. Int J Mater Sci Eng 2013;1:94–9.
[8] Khanh Tran Q, Vu Ly H, Anh Vo T, Tae Hwang H, Kim J, Kim SS. Energy Convers Manag X 2022;14:100184.
[9] Lokman IM, Rashid U, Yunus R, Taufiq-Yap YH, Taufiq- YH. Catal Rev Sci Eng 2014;56:187–219.
[10] M.K. Lam, K.T. Lee, A. Feedstocks, (2019).
[11] Feng Y, He B, Cao Y, Li J, Liu M, Yan F, et al. Bioresour Technol 2010;101:1518–21.
[12] Lokman IM, Rashid U, Taufiq-Yap YH. Meso- and Macroporous Sulfonated Starch Solid Acid Catalyst for Esterification of Palm Fatty Acid Distillate. King Saud University 2015.
[13] Sani YM, Daud WMAW, Abdul Aziz aR. Appl Catal A Gen 2014;470:140–61.
[14] Asikin-Mijan N, Lee HVV, Taufiq-Yap YHH. Chem Eng Res Des 2015;102:368–77.
[15] Rabiah Nizah MF, Taufiq-Yap YH, Rashid U, Teo SH, Shajaratun Nur ZA, Islam A. Energy Convers Manag 2014;88:1257–62.
[16] Fadhil AB, Aziz AM, Al-Tamer MH. Energy Convers Manag 2016;108:255–65.
[17] Ngaosuwan K, Goodwin JG, Prasertdham P. Renew Energy 2016;86:262–9.
[18] Abdulkareem-Alsultan G, Asikin-Mijan N, Lee HV, Taufiq-Yap YH. A New Route for the Synthesis of La-Ca Oxide Supported on Nano Activated Carbon via Vacuum Impregnation Method for One Pot Esterification-Transesterification Reaction; 2016.
[19] Niu F, Gao R, Wan X, Su K, Yue H, Dong H, et al. Int J Hydrogen Energy 2020;45:33521–31.
[20] Asikin-Mijan N, Sidek HM, Alsultan AG, Azman NA, Adzahar NA, Ong HC. Catalysts 2021;11.
[21] Alsultan A, Asikin-Mijan N, Obeas L, Islam A, Mansir N, Teo S, et al. Catalysts 2022;12:566.
[22] Zhang F, Chen J, Zhou Y, He R, Zheng K. J Lumin 2020;220:117023.
[23] Hu Y, Zhang Y, Yang C, Li J, Wang L. RSC Adv 2020;10:33080–5.
[24] Araújo AGF, Naeem M, Araújo LNM, Costa THC, Khan KH, Díaz-Guillén JC, et al. J Mater Res Technol 2020;9:14517–27.
[25] Abdulkareem-Alsultan G, Asikin-Mijan N, Mustafa-Alsultan G, Lee HV, Wilson K, Taufiq-Yap YH. RSC Adv 2020;10:4996–5009.
[26] Asikin-Mijan N, Ooi JM, AbdulKareem-Alsultan G, Lee HV, Mastuli MS, Mansir N, et al. J Clean Prod 2020;249:119381.
[27] Ibrahim SF, Asikin-Mijan N, Ibrahim ML, Abdulkareem-Alsultan G, Izham SM, Taufiq-Yap YH. Energy Convers Manag 2020;210:112698.
[28] Yang Y, Tang Z, Zhou B, Shen J, He H, Ali A, et al. Appl Catal B Environ 2020;264:118470.
[29] Zhang YS, Lu X, Owen RE, Manos G, Xu R, Wang FR, et al. Appl Catal B Environ 2020;263:118329.
[30] Shamil Albazzaz A. J. Energy Environ Chem Eng 2018;3:40.
[31] Abdulkareem-Alsultan G, Asikin-Mijan N, Taufiq-Yap YH. Key Eng Mater 2016:175–81.
[32] Goktas A, Modanlı S, Tumbul A, Kilic A. J Alloys Compd 2022;893:162334.
[33] Vogt C, Meirer F, Monai M, Groeneveld E, Ferri D, van Santen RA, et al. Nat Commun 2021;12:1–10.
[34] M. Gaithersburg, (2003).
[35] Merino NA, Barbero BP, Eloy P, Cadus LE. Appl Surf Sci 2006;253:1489–93.
[36] Fierro JLG. Catal Today 1990;8:153–74.
[37] Salam A, Abdullah B, Victor B, Ishtiaq U, Marias F, Nemitallah MA, et al. Energy Convers Manag X 2024;22:100567.
[38] Zhang X, Xu R, Liu Q, Kong G, Lei H, Ruan R, et al. Energy Convers Manag X 2022;13:100176.
[39] Haruta M, Yamada N, Kobayashi T, Iijima S. J Catal 1989;115:301–9.
[40] Richard M, Can F, Fortunato A, Diaz A, Gil S, Giroir-fendler A. Appl Catal B Environ 2017;1:2–3.
[41] Yan S, Salley SO, Simon Ng KY. Appl Catal A Gen 2009;353:203–12.
[42] Mukai D, Tochiya S, Murai Y, Imori M, Hashimoto T, Sugiura Y, et al. Appl Catal A Gen 2013;453:60–70.
[43] Najafi AM, Soltanali S, Khorashe F, Ghassabzadeh H. Chemosphere 2023;324:138275.
[44] Xu C, Zhang H, Yu S, Wu W, Zhang L, Liu Q, et al. J Mater Res Technol 2023;25:4901–12.
[45] Fan X, Ma S, Gan M, Ji Z, Sun Z, Liu L. Chem Eng J 2024;484:149636.
[46] Zhong X, Li C, Zhang L, Zhang S, Wang Y, Hu S, et al. J Environ Chem Eng 2024;12:112155.
[47] Zhang Z, Tang M, Chen J. Appl Surf Sci 2016;360:353–64.
[48] Cecilia JA, Infantes-Molina A, Rodríguez-Castellón E, Jiménez-López A, Oyama ST. Appl Catal B Environ 2013;136–137:140–9.
[49] Clark PA, Oyama ST. J Catal 2003;218:78–87.
[50] Ragupathi C, Vijaya JJ, Surendhar P, Kennedy LJ. Polyhedron 2014;72:1–7.
[51] Shah S, Sayono S, Ynzunza J, Pan R, Xu M, Pan X, et al. AIChE J 2020;66.
[52] Fonseca F. J Bras Doenças Sex Transm 2012;24:53–61.
[53] Lam SS, Wan Mahari WA, Ok YS, Peng W, Chong CT, Ma NL, et al. Renew Sustain Energy Rev 2019;115:109359.
[54] Pauletto G, Vaccari A, Groppi G, Bricaud L, Benito P, Boffito DC, et al. Chem Rev 2020;120:7516–50.
[55] Asikin-Mijan N, Lee HVV, Taufiq-Yap YHH, Abdulkrem-Alsultan G, Mastuli MSS, Ong HC. Energy Convers Manag 2016;141:325–38.
[56] Srifa A, Faungnawakij K, Itthibenchapong V, Viriya-empikul N, Charinpanitkul T, Assabumrungrat S. Bioresour Technol 2014;158:81–90.
[57] Alsultan GA, Asikin-Mijan N, Lee HVV, Albazzaz AS, Taufiq-Yap YHH, Abdulkareem-Alsultan G, et al. Energy Convers Manag 2017;151:311–23.
[58] Singha RK, Yadav A, Agrawal A, Shukla A, Adak S, Sasaki T, et al. Appl Catal B Environ 2016;191:165–78.
[59] Barros BS, Melo DMA, Libs S, Kiennemann A. Appl Catal A Gen 2010;378:69–75.
[60] A. Mukherjee, N. Sarkar, Mater. Adv. (2023).
[61] Zhou J, Zhang T, Xu Y, Zhang X. Prog Org Coatings 2023;182:107631.
[62] Signorile M, Bonino F, Damin A, Bordiga S. J Phys Chem C 2015;119:11694–8.
[63] Kubátová A, Šávová J, Seames WS, Luo Y, Sadrameli SM, Linnen MJ, et al. Energy Fuel 2012;26:672–85.
[64] Rojo-Gama D, Signorile M, Bonino F, Bordiga S, Olsbye U, Lillerud KP, et al. J Catal 2017;351:33–48.
[65] Hereijgers BPC, Bleken F, Nilsen MH, Svelle S, Lillerud KP, Bjørgen M, et al. J Catal 2009;264:77–87.